LBNL-39658
UC-404

ERNEST ORLANDO LAWRENCE
BERKELEY NATIONAL LABORATORY

Regenerative Amplification of Femtosecond Pulses: Design and Construction of a sub-100fs, μJ Laser System

A.B. Schumacher
Materials Sciences Division

October 1996
Diplomarbeit

LBNL-39658
UC-404

Regenerative Amplification of Femtosecond Pulses: Design and Construction of a sub-100fs, μJ Laser System

Andreas B. Schumacher
Diplomarbeit

Institut für Angewandte Physik der
Universität Karlsruhe, Karlsruhe, Germany

and

Materials Sciences Division
Ernest Orlando Lawrence Berkeley National Laboratory
University of California
Berkeley, California 94720

October 1996

This work was supported by the German National Scholarship Foundation and the Director, Office of Energy Research, Office of Basic Energy Sciences, Materials Sciences Division, of the U.S. Department of Energy under Contract No. DE-AC03-76SF00098.

This thesis was carried out under the supervision of:

Prof. Dr. D. S. Chemla
Department of Physics, University of California at Berkeley
Materials Sciences Division, Lawrence Berkeley National Laboratory

Prof. Dr. C. Klingshirn
Institut für Angewandte Physik, Universität Karlsruhe

at the Materials Sciences Division of the E. O. Lawrence Berkeley National Laboratory, Berkeley, CA 94720 and submitted to the Fakultät für Physik of the Universität Karlsruhe (TH).

The work was supported by the Director, Office of Energy Research, Office of Basic Energy Sciences, Materials Sciences Division, of the U. S. Department of Energy under Contract No. DE-AC03-76SF00098

Acknowledgements

My first and deepest thanks go to Prof. Daniel Chemla. During my time here, he provided me with an unbelievable amount of support and attention. I feel most privileged for having had the opportunity to work in his group.

I am deeply grateful to Prof. C. Klingshirn in Karlsruhe, who gave me the chance to come to Berkeley.

Financial support for my studies has been provided by the German National Scholarship Foundation. I am deeply indebted to them not only for funding my stay in Berkeley, but also for unforgettable summer schools and meetings.

My warmest gratitude goes to Shimshon Barad. Not only for his unending patience in teaching me how to do experiments, but even more so his friendship.

I owe special thanks to Prof. Ted Norris from the University of Michigan. He built the first Ti:sapphire regenerative amplifier and was a continuing source of ideas and help.

The work would not even have started without the steady support of Bob Schoenlein. His vast knowledge of lasers was an immeasurable help.

Thilo Enderle deserves special thanks for being a good friend and helpful advisor—both scientifcally and personally. Thanks to everybody else in the Chemla group: Jim Dunphy, Jennifer Glass, Taekjip Ha, Peter Kner, Maria-Valéria Marquezini and Shimon Weiss. All of you made my time here a very special experience. The extended MDI lunch group—Prof. Joe Orenstein, John Corson, Dave Klein, Rich Mallozzi and Gino Segrè—contributed a lot in explaining America outside LBNL.

The acknowledgements for the thesis would not be complete without my special thanks to the people outside the lab who made my time in Berkeley as pleasurable as it was. Mrs. Barbara Fritz and Kitty Pumpkin provided a home and a small family. And I shall never forget the warmth with which Ruth and Larry Nathan opened their hearts and home for me.

My deepest gratitude goes to my parents, whose love and support have been with me all my life. I dedicate this thesis to them.

And finally, thanks to Julie, the bright sun of my time here in Berkeley.

Regenerativer Titan-Saphir Laser zur Femtosekunden-Kontinuumserzeugung

Zusammenfassung

Der Einsatz von Femtosekundenlasern hat im vergangenen Jahrzehnt zu gewaltigen Fortschritten in vielen Bereichen der Physik, Biologie und Chemie geführt. Ein eigenständiges Gebiet der Spektroskopie hat sich entwickelt, in dem mit Pulsen kürzester Dauer (10^{-14}s) Nicht-Gleichgewichtszustände der Materie und fundamentale Gesetze der Quantenmechnik untersucht werden können.

Während die Grenzen für Pulsdauer und -energie weiter hinausgeschoben wurden, stehen andererseits immer handlichere und zuverlässigere Systeme zur Verfügung. In den meisten Fällen ist der zur Verfügung stehende Spektralbereich dieser Laser jedoch begrenzt. Zwar ermöglichen es Laser mit austauschbaren Farbstoffen, diese Einschränkungen teilweise zu umgehen. Die gleichzeitige Untersuchung von Prozessen, die in einem weiten Spektralbereich ablaufen, ist aber auch mit ihnen nicht möglich.

Diese Arbeit beschreibt die Berechnung, den Aufbau und die Charakterisierung einer Femtosekunden-Lichtquelle, mit der derartige spektrale Beschränkungen umgangen werden können. Es wird gezeigt, wie die Ausgangspulse eines moden-gekoppelten Titan:Saphir Lasers zu μJ Energien verstärkt werden können. Dabei bleiben die Pulse kürzer als 100fs. Eine Kombination von kontinuierlichem Pumpen, akusto-optischen Schaltern und Ti:Al_2O_3 als Verstärkermedium erlaubt eine hohe Pulswiederholungsfrequenz. Durch Fokusierung der energiereichen Pulse in ein Saphirkristall läßt sich ein breitbandiges Kontinuum erzeugen, das sich über mehrere hundert Nanometer erstreckt.

Um eine Verstärkung der Pulsenergie um drei Größenordnungen unter Beibehaltung der Pulsdauer zu erreichen, wurde ein regenerativer Laserverstärker aufgebaut. Das System (insbesondere der optische Resonator des Verstärkers) wurde im Rahmen dieser Arbeit berechnet, gebaut und getestet. Die unabhängige Untersuchung wichtiger Einzelkomponenten er-

laubte darüber hinaus, Rückschlüsse auf die Leistung des Gesamtsystems zu ziehen.

Ein moden-gekoppelter Ti:Saphir Laser liefert die Ausgangspulse für den Verstärker. Bei einer Pulsenergie von einem Nanojoule sind sie um 100fs (nicht bandbreitenbegrenzt) lang. Vor Einkopplung in den Verstärker wird die Pulsdauer auf über 50ps gestreckt, um nichtlineare optische Effekte und Materialbeschädigung zu vermeiden. Ein außschliesslich aus Reflektionsoptik aufgebauter Gitterstretcher minimiert chromatische Abberation. Anschließend passieren die Pulse einen Faraday-Isolator und werden mit einem akusto-optischen Schalter in den optischen Resonator des Verstärkers eingekoppelt.

Die astigmatisch kompensierte Kavität enthält ebenfalls einen Ti:Saphir-Kristall als aktives Medium. Seine kurze Energiespeeicherzeit in Verbindung mit dem kontinuierlichen Pumpem durch einen Argon-Ionen Laser bilden die Grundvoraussetzung fuer die hohe Puls-Wiederholungsfrequenz des Systems. Um während des Pumpvorgangs eine möglichst hohe Inversionsdichte im Lasermedium erzeugen zu können, muß spontanes Lasen des Verstärkers vermieden werden. Ein zweiter akusto-optischen Schalter setzt deshalb die Güte der Kavität herab. Unmittelbar vor Einkopplung eines Pulses in den Verstärker wird deren ursprüngliche, hohe Wert wieder hergestellt. Nach 50-60 Umläufen im Resonator hat der eingekoppelte Puls die Inversion im Lasermedium abgebaut und wird aus dem Verstrker ausgekoppelt. Eine abschließende Pulskompression ist notwendig, um den Einfluß des Stretchers und Materialdispersion ausgleichen zu können. Eine Rück-Kompression auf unter 100fs konnte erfolgreich demonstriert werden.

Neben dem optischen und mechanischen Design beschreibt die Arbeit den Aufbau der Steuerungselektronik. Hier misßt eine schnelle Photodiode die moden-gekoppleten Ausgangspulse des Lasers. Nach einer elektronischen Aufbereitung triggert das Signal die "Hauptuhr" des Verstärkers. Letztere steuert dann die Ein- und Auskopplung von Pulsen in den Verstärker sowie die Güteschaltung der Kavität.

Abstract

Femtosecond lasers are a powerful tool for a wealth of applications in physics, chemistry and biology. In most cases, however, their use is fundamentally restricted to a rather narrow spectral range. This thesis deals with the construction and characterization of a femtosecond light source for spectroscopic applications which overcomes that restriction.

It is demonstrated how the output of a continuously pumped Ti:sapphire femtosecond oscillator is amplified to the μJ level, while the pulse duration remains below 100fs. A combination of continuous pumping, acousto-optic switching and Ti:Al_20_3 as a gain medium allows amplification at high repetition rates. By focusing the high energy pulses into a sapphire crystal, a broad-band continuum can be generated, extended in wavelengths over several hundred nanometers.

To accomplish amplification of three orders of magnitude while maintaining the pulse length, a regenerative multipass amplifier system was built. The thesis describes theoretical design, realization and characterization of the system. Theoretical calculations and preliminary measurements were carried out and allow a critical evaluation of the final performance.

Contents

List of Figures

Chapter I

Introduction

I.1 Motivation

Femtosecond lasers have rapidly gained recognition as powerful tools in research. While limits for pulse duration and energy have been pushed further, the systems have become more compact and easier to handle. This gave rise to a wealth of new scientific fields in physics, chemistry and biology (see i.e. [39]) A new era of spectroscopy has emerged, with pulses so short that one can examine non-equilibrium states of matter or test fundamental quantum and light interactions [5, 6, 12, 75, 86, 87].

In most cases, however, research with ultrashort light pulses is restricted to a rather narrow spectral range. The limitations are imposed by the emission spectrum of the laser media. At the expense of pulse duration, lasers with exchangeable dyes ease those restrictions somewhat. Nevertheless, they remain inconvenient to handle.

A highly nonlinear optical process called "continuum generation" [2] allows to overcome all the problems: The interaction between a strong transient electrical field of a laser and matter can cause the pulse frequency to sweep over a wide spectral range. This creates a broadband (hundreds of nanometers), essentially "white light" laser pulse [3].

The necessary short, high energy pulses can not be created directly from a laser cavity; an amplifier—which preserves the pulsewidth—is needed. This thesis describes the construction of an ultrashort pulsed, fast regenerative amplifier system. It is capable of delivering sub-100fs pulses at high repetition rates and of sufficient energy to create continuum.

The fundamental principles for the generation of ultrashort optical pulses were discovered during the very first years after the invention of the laser [17, 25, 82, 89]. Since 1966, when the first pulse in the picosecond range were reportet, dramatic decrease in pulse length has taken place [16, 20]. The shortest pulses created up to date have a duration of 6fs, which corresponds to merely 3 cycles of the electromagnetic field at 620nm [18] But only since 1991, when the first mode-locked Titanium:Sapphire laser was built [78], a reliable solid-state femtosecond laser is available. Recent design improvements allow to obtain sub-10fs pulses directly from a resonator [48], thus approaching the gain bandwidth limit of Ti:$Al_2 0_3$.

At the same time, there has been substantial interest in increasing the pulse energy from short pulsed lasers. Typically, multi-stage, multi-pass systems are used to boost the pulse energy in several steps [61]. At low repetition rates, energies >1J for 15fs pulses have been demonstrated, which pushes the peak power towards the peta (10^{15}) watt level.

For spectroscopic applications, however, only much lower pulse energies are needed. More desirable are high repetition rates to allow experiments with good signal-to-noise ratio. For most amplifiers, the repetition rate is limited by either the pump laser or the pulse switching mechanism. The first system to overcome both limitations still emitted picosecond pulses [67]. It was pumped continuously and facilitated fast, acousto-optical switching. The very same concept was applied in 1992 to Ti:sapphire by T. Norris [37, 58, 77]. The short energy storage time of Ti:$Al_2 0_3$ made it possible to efficiently extract pulses up to several hundred kilohertz. At the same time, the pulse energy remained high enough to create a stable broad-band continuum. The useful spectral range has been further extended by generation of harmonics and parametric oscillators [63–65].

The process of spectral superbroadening—or "continuum generation"—was first studied 1969 [3]. In this highly nonlinear optical process, the interaction between the laser pulse and a sample causes the frequency of the laser radiation to sweep over a wide spectral range. With laser pulses becoming shorter over the years, it became possible to create continua in the uv-, visible and infrared spectral region. Furthermore, continua have been observed in a large variety of gaseous and solid media. For the field of spectroscopy, continuum generation offered a long sought after solution: High temporal resolution is combined with the opportunity to detect sample responses over a wide spectral range.

I.2 Research Objectives and Overview

The goal of the thesis was to provide a femtosecond, high energy light source which could later be used for continuum generation and spectroscopic applications. Therefore, a regenerative amplifier system, capable of producing sub-100fs, μJ pulses at high (100-200kHz) repetition rates was built.

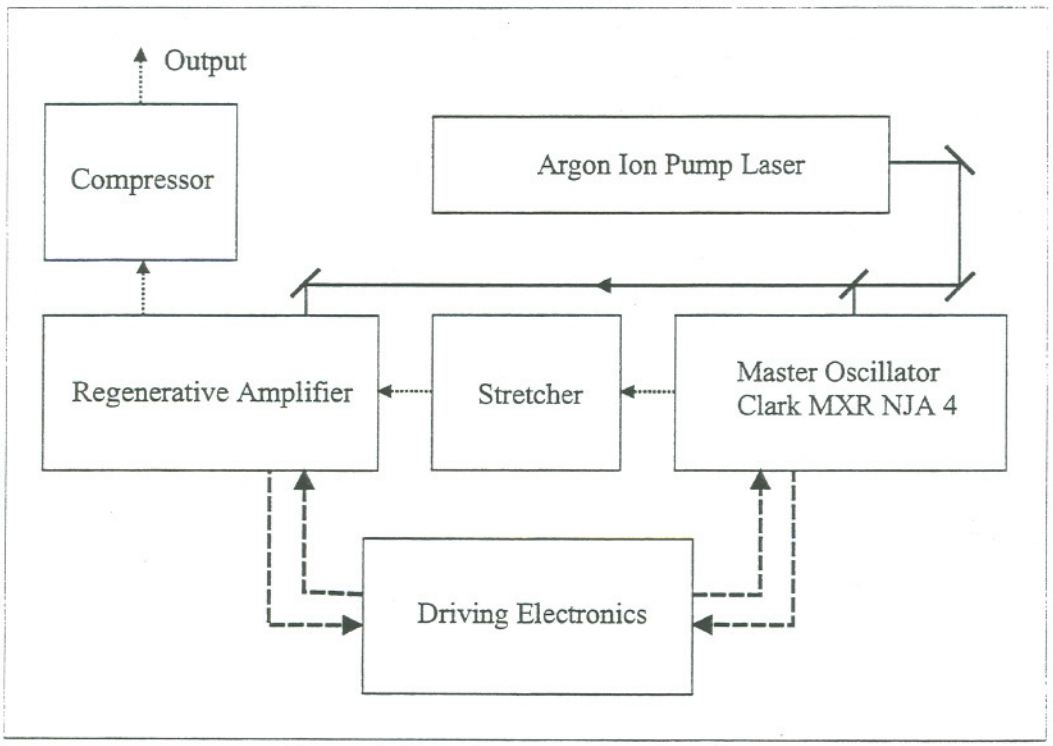

Figure I.1: Schematic setup of a Ti:sapphire oscillator-amplifier system.

Fig I.1 shows a schematic diagram of the laser-amplifier system. A mode-locked Ti:sapphire laser serves as the master oscillator. It provides sub-100fs pulses at a repetition rate of 113MHz. Prior to injection into the amplifier, the fs pulses are stretched to more than 50ps. This is essential to avoid nonlinear effects and optical damage in the amplifier. After several cavity round-trips and an amplification of three orders of magnitude, the pulses are extracted out of the system. Acousto-optic switching is used to obtain high repetition rates of 150-250kHz. A final recompression is needed to compensate for the effect of the stretcher and the dispersion in the amplifier.

The pulse width is again reduced to ≈100fs. With an energy of more than 1μJ after amplification, continuum generation is possible.

The structure of the thesis is as follows: After the introduction, chapter II describes the design of an astigmatically compensated cavity for the regenerative amplifier. *ABCD*-Matrices and Gaussian beams are introduced. Astigmatism and its significance for resonator design are pointed out. The chapter concludes with a simulation of the final cavity.

Chapter III gives an overview of Ti:sapphire lasers and Ti:Al_2O_3 as a gain medium. An explanation for Q-switching and mode-locking is given. Experimental results are obtained which verify proper performance of the amplifier cavity and the Ti:Al_2O_3 crystal.

Chapter IV deals with pulse compression and stretching. We review the underlying theory and present the system which we use. The performance of the stretcher/compressor combination is analyzed experimentally.

In chapter V , the integration of all parts into a complete system is described. To understand the mechanism of acousto-optic switching, it is explained separately. Driving electronics and the optical setup are presented. We conclude by discussing the final amplifier parameters. An outlook and suggestions for improvements are given.

Since the system will ultimately be used to generate continuum, this topic is discussed in an appendix.

Chapter II

Cavity Design

The cavity forms the optical resonator of a laser system, thus providing the feedback for light amplification. Furthermore, the design of the cavity determines stability regions, mode structure, loss mechanisms and other important parameters. The goal of this chapter is to review theoretical concepts of cavity design with a focus on the system described in this thesis.

The first section describes the passage of paraxial rays through optical elements. It explains the concept of *ABCD* - or *Ray Transfer* Matrices. The Gaussian beam expression, as the lowest-order solution for the free-space paraxial wave equation, is then introduced. Combining these two concepts allows one to calculate the beam parameters at any given point inside the amplifier cavity.

In the second section, the theory is extended to astigmatic Gaussian beams which are produced by axially asymmetric laser cavities. These departures from the idealized paraxial condition lead to the concept of the *astigmatically compensated* cavity. Every laser design for linearly polarized lasers follows this idea, since any Brewster-cut element inevitably causes a loss of axial symmetry. Together with the results of the first section, it is then possible to fully evaluate the beam parameters in the resonator of the regenerative amplifier.

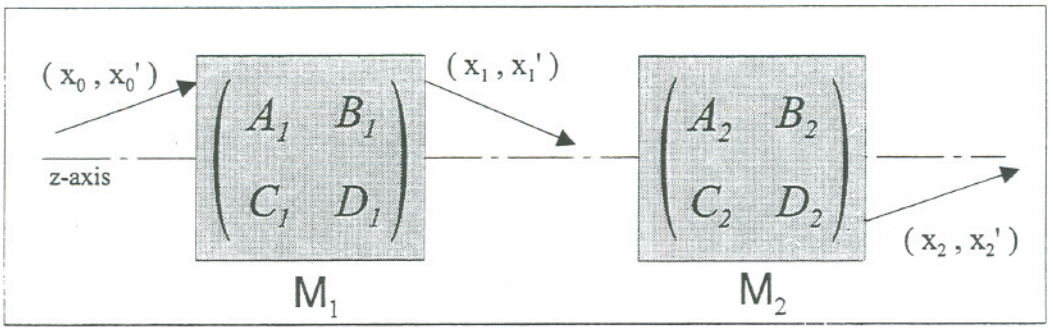

Figure II.1: Ray transformation through optical elements

II.1 Paraxial Ray Analysis

Studying the passage of a paraxial ray through an optical system can reveal important information about it. Examples include the stability of the structure [8] and the loss of unstable resonators [72]. In this first section, the treatment is restricted to the case of cylindrical symmetry. A much more detailed review of the subjects described below can be found in the paper of Kogelnik and Li [45] or in a number of textbooks about lasers [73]

II.1.1 *ABCD*-Matrices

A paraxial ray at a given position $z = z_0$ along the optical axis can be described as shown in Fig. II.1. The distance from the optical axis is x_0 and x_0' its angle or slope with respect to it. After passing through an optical element, the ray is determined by x_1 and x_1'. In the paraxial limit, the output quantities depend linearly on the input quantities. This can be written conveniently by using the *ABCD*-Matrix M of the element.

$$\begin{pmatrix} x_1 \\ x_1' \end{pmatrix} = \begin{pmatrix} A & B \\ C & D \end{pmatrix} \cdot \begin{pmatrix} x_0 \\ x_0' \end{pmatrix}$$

Examples for matrices describing different optical elements can be found in [73].

For a system consisting of n optical elements, the total ray matrix M_{tot} is given by

$$\mathsf{M}_{tot} \equiv \mathsf{M}_n \mathsf{M}_{n-1} \cdots \mathsf{M}_2 \mathsf{M}_1$$

An optical resonator is an example for a *periodic focusing system*, e.g., a combination of elements in which the same sequence is repeated many times.

Such a system can be classified as either *stable* or *unstable*, depending on whether the rays remain confined to a finite region around the z-axis or not. The task of finding the stability conditions for a resonator transforms into retrieving stable solutions for:

$$\mathbf{x}_{n+1} = \mathsf{M}_{tot}\mathbf{x}_n = \mathsf{M}_{tot}^{n+1}\mathbf{x}_0, \tag{II.1}$$

with $\mathbf{x}_n = (x_n\,,\, x_n')$ and M_{tot} =ray matrix for one round trip through the cavity.

Such a problem is analyzed by calculating the eigenvalues and eigensolutions of M_{tot}. Defining the angle ϕ and according to [73] the "m parameter" as

$$\cos\phi \equiv \frac{A+D}{2} \equiv m,$$

the eigenvalues can be written

$$\boxed{\lambda_a, \lambda_b = m \pm i\sqrt{1-m^2} = \cos\phi \pm i\sin\phi = e^{\pm i\phi}} \tag{II.2}$$

With the corresponding eigenvectors $\mathbf{x_a}$ and $\mathbf{x_b}$, the propagation of any ray can then be expressed as

$$\mathbf{x_n} = c_a\mathbf{x_a}e^{+i\phi} + c_b\mathbf{x_b}e^{-i\phi}, \qquad c_a, c_b = const. \tag{II.3}$$

It can be readily seen that stable solutions exist only for $|m| < 1$. If $|m| > 1$, the eigenvalues become real, and $\{|\mathbf{x_n}|\}$ has no upper limit if $c_a, c_b \neq 0$. Therefore, an important stability criteria for resonators is:

$$\boxed{\text{A laser cavity is stable if } \tfrac{1}{2}|Tr(\mathsf{M}_{tot})| < 1} \tag{II.4}$$

II.1.2 Paraxial Wave Equation and Gaussian Rays

Whereas in the preceding part only geometrical considerations were of importance, this paragraph deals with the wave nature of light. A monochromatic electromagnetic field in free space is governed by the equation:

$$\nabla^2 u + k^2 u = 0, \qquad k = \tfrac{2\pi}{\lambda} \tag{II.5}$$

For the case of an electromagnetic wave inside a laser resonator, some simplifications can be made. Of primary interest is a solution which describes a

traveling wave in the direction of the optical axis z. The spatial dependence of $u(x,y,z)$ on z is therefore an $\exp\{-ikz\}$. Compared to this spatial period of one λ, the variation in the x,y-direction is rather slow. Thus it can be written:

$$u(x,y,z) = \psi(x,y,z) \cdot e^{\{-ikz\}}, \tag{II.6}$$

where ψ is a slowly varying function which describes the difference between $u(x,y,z)$ and a plane wave. These differences are: a.)a slow spatial variation in x,y-direction and b.) variations of both the intensity and phase profile with the expansion of the beam (the differences will be discussed in more detail below). We now use (II.6) to solve (II.5) and keep in mind the above assumptions. This leads to the so called *Paraxial Wave Equation* (in rectangular coordinates) [15] for ψ:

$$\frac{\partial^2\psi}{\partial x^2} + \frac{\partial^2\psi}{\partial y^2} - 2ki\frac{\partial\psi}{\partial z} = 0. \tag{II.7}$$

The equation is solved by

$$\psi = \exp\left\{-i\left(P + \frac{k}{2q}\cdot r^2\right)\right\}, \qquad r^2 = x^2 + y^2. \tag{II.8}$$

Inserting (II.8) into (II.7) yields two equations for the *complex phase shift* P and the *complex beam parameter* q

$$\frac{dP}{dz} = \frac{-i}{q} \quad \text{and} \quad \frac{dq}{dz} = 1 \tag{II.9}$$

It is convenient to define the two real quantities R and w by

$$\frac{1}{q} \equiv \frac{1}{R} - i\cdot\frac{\lambda}{\pi\cdot w^2}, \tag{II.10}$$

which finally leads to the propagation law for Gaussian beams

$$\boxed{\psi = \exp(-iP) \times \exp\left\{-i\frac{kr^2}{2R}\right\} \times \exp\left\{\frac{-r^2}{w^2}\right\}} \tag{II.11}$$

The equation illustrates the meaning of R and w. The latter is a measure of the beam radius, and R gives the radius of curvature of the phase front.

A number of useful relations describing the spatial beam evolution can be extracted from equations (II.11) and (II.10) [73]. We set the center of the coordinate system to a point where the wavefront is planar ($R_0 = \infty$) in the transverse direction. Then, (II.10) is used to define a parameter z_R:

$$q_0 \equiv \quad i\pi\frac{w_0^2}{\lambda} \quad \equiv i \times z_R \qquad \text{and} \tag{II.12}$$

$$q(z) = \quad q_0 + z \quad = i \times z_R + z \tag{II.13}$$

A comparison with real- and imaginary parts of (II.10) leads to the useful expression:

$$\boxed{w(z) = w_0\sqrt{1 + \left(\frac{z}{z_R}\right)^2}.} \tag{II.14}$$

Finally, it should be noted that (II.11) describes a TEM_{00}-mode. This is the lowest order solution of the wave equation. Other modes of propagation, which form a set of complete and orthogonal functions, do exist [45, 73]. These higher modes contain generalized Laguerrian polynomials in cylindrical coordinates and Hermite polynomials in rectangular coordinates. Expression (II.11) is a special case of the latter ones.

II.1.3 Laser Resonators with Infinite Aperture

The combination of the ray transfer matrices and the propagation law (II.9) finally allows one to calculate the beam profile inside a laser cavity.

It can be shown [73] that a Gaussian beam passing through an arbitrary optical element with a given $ABCD$-Matrix undergoes the transformation:

$$\frac{1}{q_1} = \frac{A\,q_0 + B}{C\,q_0 + D} \tag{II.15}$$

This relation is called the $ABCD$-Law [43]. To calculate the mode structure of a cavity, one requires the complex beam parameter to repeat itself after a given number (usually one) of round trips: $q_1 = q_0 \equiv q$. By using the matrix elements of the complete cavity M_{tot} and solving the resulting quadratic equation, one obtains:

$$\frac{1}{q} = \frac{D - A}{2B} \pm \frac{i}{2B}\sqrt{4 - (A + D)^2}, \tag{II.16}$$

which yields for the corresponding beam radius w,

$$\boxed{w^2 = \frac{2\lambda B}{\pi} \cdot \sqrt{4 - (A+D)^2}.} \tag{II.17}$$

To obtain the complete beam profile along the optical axis, (II.16) has to be solved for different values of z. The z dependence of the right-hand side of both equations is given through the matrix elements of M_{tot}, which change along the axis.

It should be noted that this description neglects edge effects like diffraction and is therefore valid only in the limit of an infinitely wide resonator. Aperture effects require a different treatment [45].

II.2 Astigmatic Laser Cavities

In the above section, axial symmetry for all optical elements was assumed. This is true, however, only in some cases. A Brewster-cut rod, or a curved mirror which reflects obliquely, cause a loss of this symmetry. In many cases, it is nevertheless possible to analyze the ray behaviour in each transverse coordinate separately and independently. Such systems, which can be described by two different ray matrices in two perpendicular principal planes, are called *orthogonal systems*. In the more general *nonorthogonal* case, where operations such as arbitrary astigmatism or image rotation can be treated, an extension of the ray-transfer matrix method is necessary [73]. For this thesis, it is sufficient to introduce two ray matrices for tangential and sagittal plane[1]. All beam parameters are then calculated for the two planes independently. This can be justified mathematically since all the expressions for Gaussian beams are separable in the x and y coordinates. The argument holds true for higher-order solutions of the paraxial wave equation as well.

Different solutions for the tangential and sagittal plane are not only of theoretical interest. One example, which is discussed below, affects the stability of the laser: As it will be shown, a cavity can be stable in both planes independently, but the stability regions do not overlap. In such a configuration, lasing would no occur.

[1] The tangential plane contains the chief ray and the optical axis; the sagittal plane is perpendicular and also contains the chief ray [31]

II.2.1 Astigmatic Elements

Two types of astigmatic elements are used in the regenerative amplifier: curved mirrors and Brewster-cut crystals. Their influence on the intracavity beam profile is outlined here. The propagation of a Gaussian beam through these elements is discussed.

Mirrors

It is known [33] that a mirror used at oblique incidence focuses sagittal ray bundles at a different location than tangential ray bundles. This can be expressed by two different focal lengths f_{yz} and f_{xz}. They are related to the focal length f_0 at normal incidence by

$$f_{xz} = f_0/\cos\Theta \quad \text{and} \quad f_{yz} = f_0 \times \cos\Theta, \tag{II.18}$$

where Θ is the angle of incidence. The result can be readily taken over into the $ABCD$-formalism, since tangential (yz) and sagittal (xz) plane are now treated separately.

Beam propagation through a Brewster plate

Consider a Gaussian beam being incident at an angle α_B on a transparent parallel-sided plate as shown in Fig. II.2. This plate has a thickness t, index of refraction n and is perpendicular to the yz-plane.

First, it can be shown with simple geometrical optics that the beam is shifted by

$$d = t \times \left(1 - \frac{\cos\alpha_B}{n\cos\alpha_n}\right)(\sin\alpha_B). \tag{II.19}$$

Next, we want to investigate the spatial development of the beam *inside* the plate. We look at an axially symmetric beam with a waist w_0 just at the surface of the inclined plate. A simple geometrical projection shows that only the beam waist in the xz-plane remains unchanged upon entering the plate, whereas the waist in the yz-plane increases. The necessary factor can be derived using Snell's law[2]:

[2]To agree with the literature, the subscript xz is kept for parameters in the sagittal plane. Strictly speaking, this would require a rotation of the coordinate system around the x-axis

$$w_{xz} = w_0 \tag{II.20}$$
$$w_{yz} = w \times \left.\frac{\cos\alpha_n}{\cos\alpha_B}\right|_{\alpha_B=Brewster\ angle} = n \times w_0$$

The result has a significant impact on solid state lasers with a Brewster cut active laser medium: Even if the astigmatism outside the rod is negligible, the spot size inside the a Brewster-cut laser rod is $n\times$ larger in the yz-plane. Consequently, the mode volume in TEM_{00} operation is $n\times$ larger compared to normal incidence. This enhances energy extraction and relaxes problems of material damage.

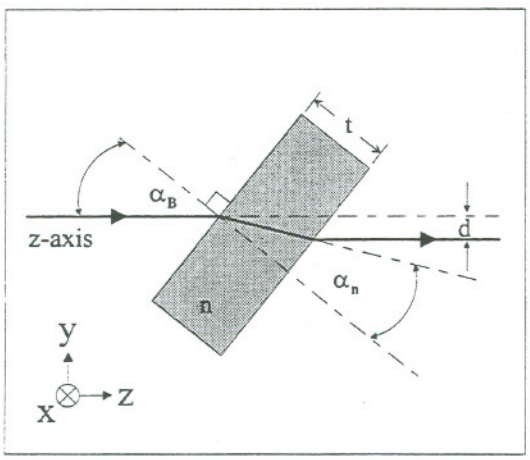

Figure II.2: Beam propagation through an inclined plate

Another consequence of the different spot sizes emerges from the equation for the spatial development of the beam radius (II.14). With two different waists $w_{0,xz}$ and $w_{0,yz}$ the evolution of $w(z)$ is no longer the same in both planes. Hanna [24] found an elegant description for this case. By simply applying the propagation laws for Gaussian beams, he showed that (II.11) can still be used if the optical pathlength is modified for both tangential and sagittal plane. The two new lengths ϱ_{yz} and ϱ_{xz} are:

$$\varrho_{yz} = \frac{t}{n^3 \sin\left(\tan^{-1} n\right)} \tag{II.21}$$
$$\varrho_{xz} = \frac{t}{n \sin\left(\tan^{-1} n\right)} \tag{II.22}$$

As a consequence of the different length scales in different planes, the beam shape becomes oval. In general it is no longer possible to speak about only one focal point inside a Brewster-cut plate. That is a major point of concern

whenever one is interested in a very small beam volume $V = \int \pi w_{xz} w_{yz} dz$ inside a crystal. Kogelnik *et al.* [44] found an analytical expression for the beam cross-section. They also showed that the beam volume inside the Brewster element can be minimized if the two beam waists are equidistant with respect to the center of the crystal.

Fig. II.3 shows results of own calculations. The influence of crystal thickness and focusing for the Ti:Sapphire crystal used in the regenerative amplifier (a) and in a new 15fs-laser (b) are compared. The goal is to simulate the focusing of the pump beam into the regenerative amplifier. In both cases, no major influence of the additional Brewster plate can be observed for a spot size of 25μm. This number is of special interest, since it will turn out to be the size of the intracavity beam of the amplifier cavity.

Fig. II.3 reveals another interesting fact: There is a limiting effect of the cell thickness on the achievable minimum beam concentration. Only in the case of the thin cell (b), a tighter focusing leads to a decreasing beam area. For the 20mm crystal, a double minimum develops and the cross section between them increases again. Whether case (a) or (b) applies, depends on the ratio between confocal parameter z_R and cell thickness t. In the limit of a large thickness $t \gg z_R$, it was found [44]

$$A \sim \lambda t(n^2 - 1)/n^3\sqrt{n^3 + 1} \qquad \text{(II.23)}$$

For titanium- doped sapphire ($n = 1.76$), this limit is approximately $A = \frac{1}{4}\lambda t$

II.2.2 Astigmatically Compensated Cavity

The outlined astigmatic properties of lenses and Brewster plates raise an important question for the design of lasers cavities:

> Since tangential and sagittal plane in an astigmatic laser cavity have to be treated independently, different stability regions are likely to occur. How can one design and optimize a cavity which is stable in both planes?

The solution was given in the paper by Kogelnik *et al.* [44] and later improved by Johnston and Runge [83]. The derivation refers to a laser cavity as shown in Fig. II.4. Such a design is of great practical interest. In many cases, there is a need for cavities with an intracavity focus. Pumping requirements or acousto-optical interactions such as Q-switching or cavity dumping are

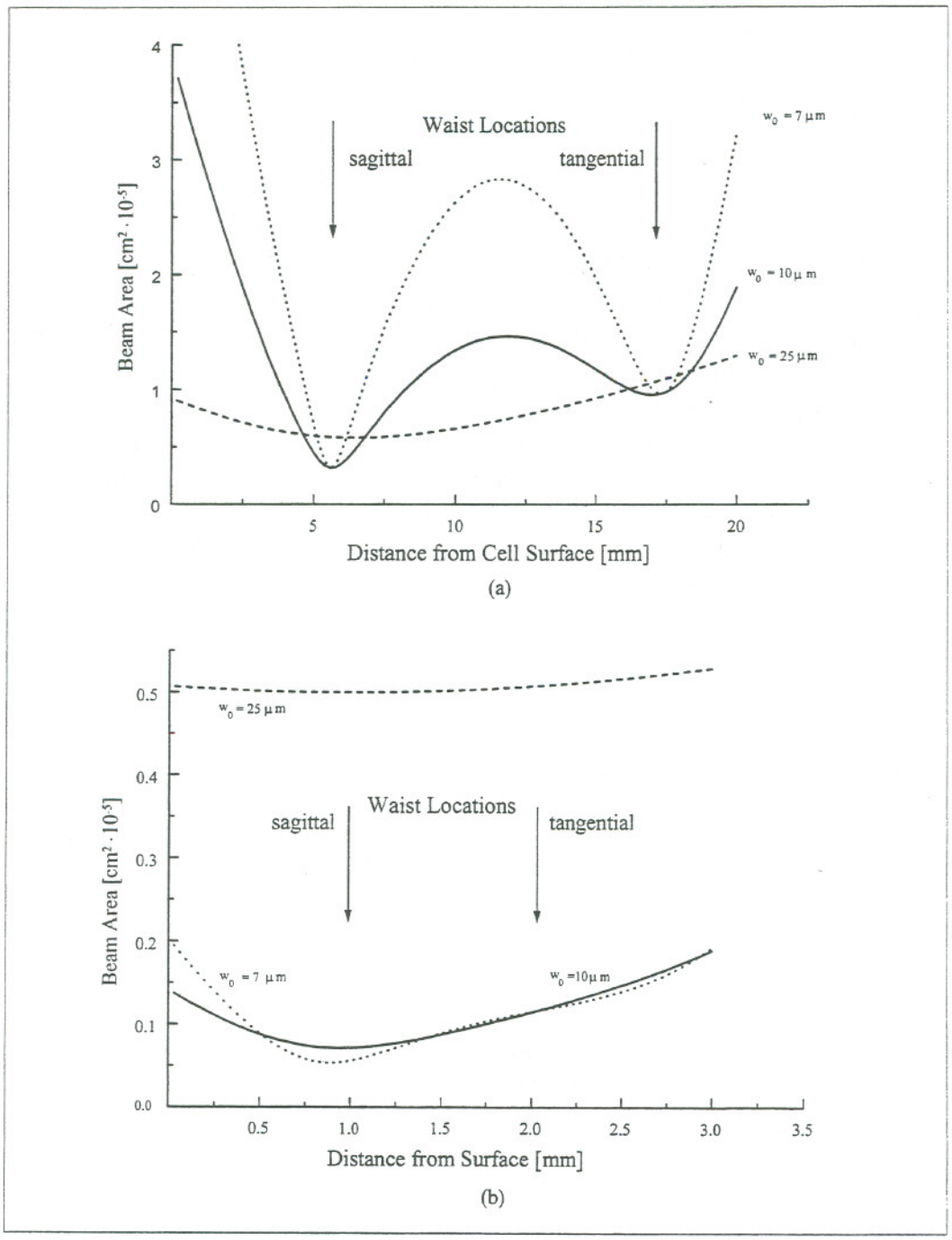

Figure II.3: Gaussian beam propagation through a Brewster plate. $\lambda = 820$nm, $n = 1.76$. (a) $t = 20$mm. (b) $t = 3$mm. The indicated waist sizes are values for assumed focusing in air.

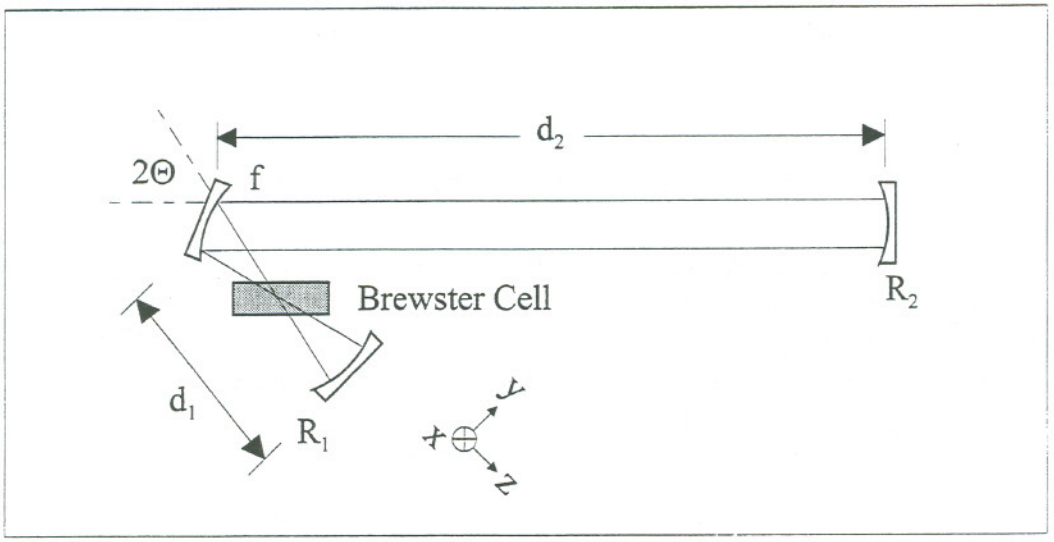

Figure II.4: Folded 3-mirror cavity with internal Brewster-angle cell of thickness t. $d_2 \gg d_1$ and $d_1 \approx R_1 + f$

two examples where a high transversal beam concentration is required. For tuning and mode-locking, a fairly long overall cavity length is desired. To avoid chromatic abberations and high insertion losses, resonators like this oneare usually build out of all-reflective optics, rather than using intracavity lenses. This, on the other hand, causes astigmatism at the center mirror. Additional astigmatism is caused by the Brewster element, which has to be inserted for all the above applications (laser rod, acousto-optical crystal).

The idea of an astigmatic compensation is to provide a maximum overlap between the stability regions for tangential and sagittal plane. Kogelnik *et al.* found this condition to be satisfied if

$$\boxed{2Nt = 2f \sin\Theta \tan\Theta \equiv R \sin\Theta \tan\Theta} \qquad \text{(II.24)}$$

where $N = (n^2 - 1)\frac{\sqrt{n^2+1}}{4}$ and n is the index of refraction.

But even after adjusting the angles correctly, the problem of the different waist locations inside the Brewster-cut element remains. W. Johnston and P. Runge [83] therefore suggested an important improvement to the design Fig. II.4. By simply "doubling" the cavity to a "z" shaped configuration, symmetry forces the major and minor axis of the elliptical beam waist to be simultaneously minimum at the same spatial position. The mathematical treatment of this configuration is similar: Each off-axis mirror is associated

with half the thickness of the brewster-crystal, and equation (II.24) remains valid.

II.3 Regenerative Amplifier Cavity

The cavity of the regenerative amplifier needs two intracavity focal points: One for the Ti:$Al_2 0_3$ crystal and a second one for the pulse switching mechanism, an acousto-optic crystal. Together with the Q-switch (which will be described later), there are three Brewster-cut plates inside the resonator. To obtain astigmatic compensation, the angles and distances between the elements of the cavity have to be chosen carefully.

To obtain accurate results, we calculated the overall $ABCD$-Matrix of the system with an optical design program. Eq. (II.4) then had to be evaluated for different angles Θ and the overlap between the stability regions maximized.

Fig. II.5 displays the resulting stability map for our specific amplifier cavity. All the optical elements were considered. The plot shows the stability of the system as a function of cavity folding angle and length of the the distance between the surface of Ti:sapphire crystal and the enclosing focusing mirrors. All other parameters remain unchanged.

The two vertical lines illustrate the difference between the simple equation (II.24) and the complete Matrix analysis. Line (a) marks the angle at which the overlap between the stability regions is maximized according to the matrix-method (31.8°). Line (b) shows the result of (II.24). It is noteworthy that (II.24) models only a simple, "z"-folded cavity with no intracavity elements other than the laser rod. Nevertheless, the results agree remarkably well. A cavity built according to equation (II.24) would allow stable operation—but with a smaller adjustment range. From the graph it can also be extrapolated that for cavity folding angles $> 45°$, no stable operation is possible. This was indeed found; a cavity built with $2\Theta = 50°$ did not lase.

Finally, Fig.II.3(a) and II.3(b) show the complete amplifier cavity. It is astigmatically compensated and provides two foci for pumping and cavity dumping, with the spot sizes matched for these purposes. The position of the Q-switch is uncritical. The intracavity beam profile is calculated by using (II.16). The $n\times$ increase of the waist size in the Q-switch for the tangential plane can be clearly seen. Also, since the cavity is not exactly symmetrical, the waist locations inside the Ti:Sapphire crystal are slightly different for

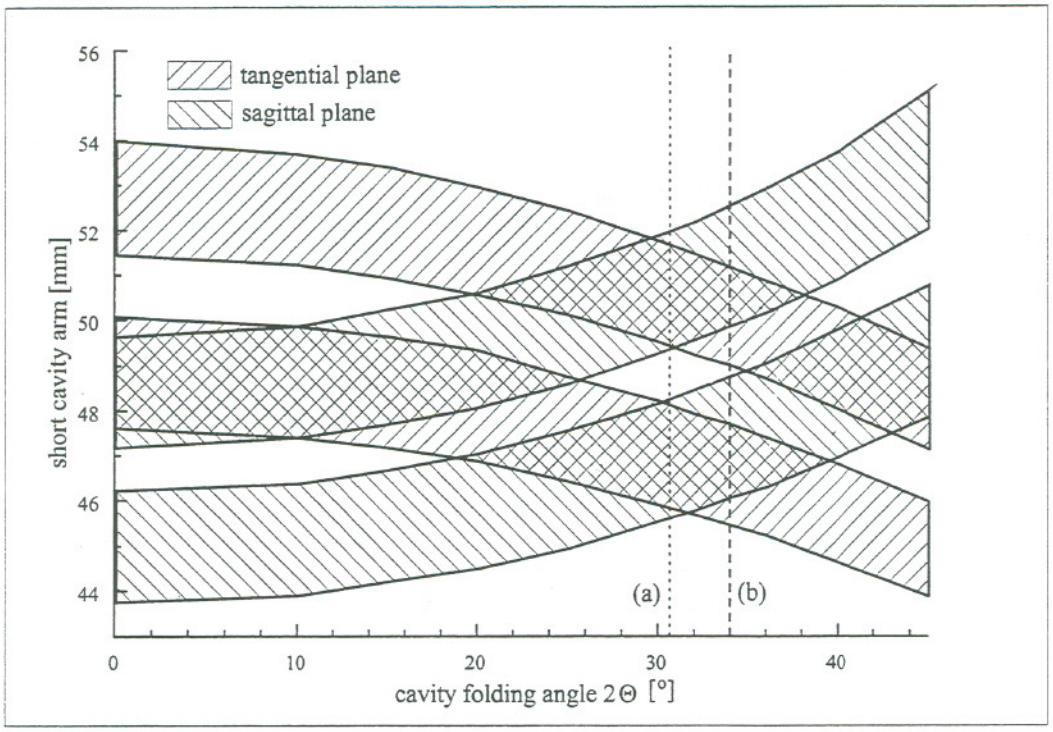

Figure II.5: Stability map for the cavity of the regenerative amplifier

xz and yz plane. For both focal points, the difference in the waist sizes is smaller than 10%. The numbers given in the graph are averaged.

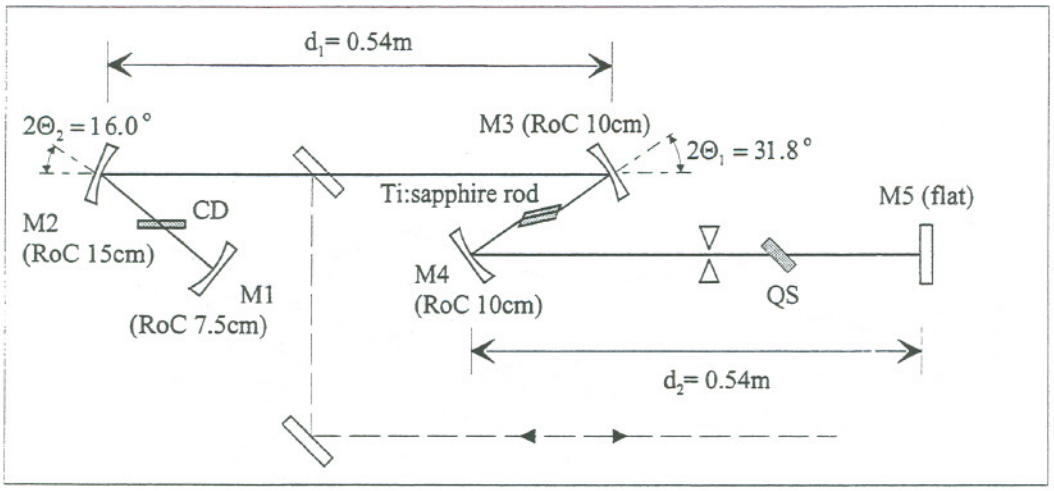

Figure II.6: Diagram of the final amplifier cavity. The path of the injected and cavity dumped pulses is drawn dashed. CD=cavity dumper, QS=Q-switch, M1-M5=mirrors. The distance between the Ti:Al_2O_3 rod and M3, M4 is 4.7cm

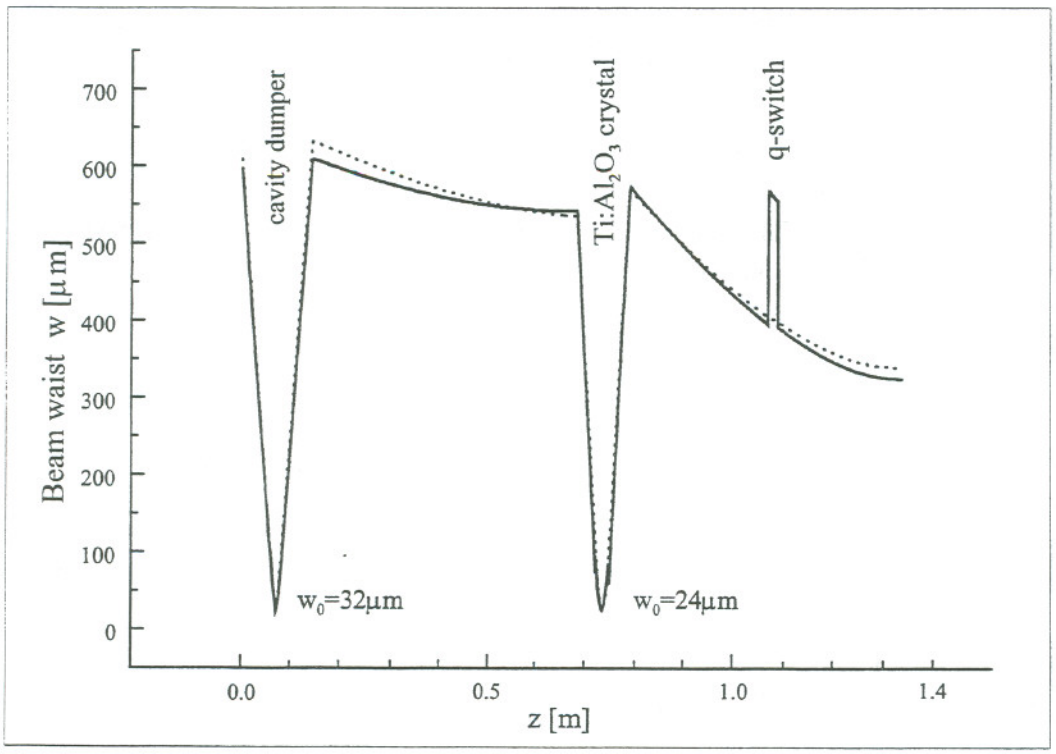

Figure II.7: Final intracavity beam profile. Solid line=tangential plane, dashed line=sagittal plane

Chapter III

Ti : Sapphire Lasers

A regenerative amplifier belongs to the class of *resonator amplifiers*. In these systems, a medium with only a moderate single-pass gain is placed inside a stable optical resonator. The desired large overall gain is then obtained through multiple round trips in this cavity. To verify the stability of the amplifier resonator, the amplifier itself is first operated as an independent laser. This presents the advantage of giving experimental access to fundamental laser parameters, such as loss, gain and mode structure.

The first section focuses on the properties of the gain medium. Ti:sapphire is widely used for both tunable and ultrafast lasers. Vibronical broadening—the mechanism which is responsible for the exceptionally wide tuning range of some lasers—is explained. Optical parameters of importance for the amplifier are discussed. Among those are the absorption and the single-pass gain of our Ti:Al_20_3 crystal.

The second section deals with the independent laser operation of the cavity. Within the vast field of laser theory, we have to restrict our attention to a few selected problems. We therefore concentrate on pulsed lasers. The main concepts of Q-switching and mode-locking are outlined.

Results of characterization experiments are given in the last section, together with an illustration of the methods. In addition, the master oscillator, which is used for seeding the amplifier, is described briefly.

III.1 Ti : Sapphire as Gain Medium

Already in the introduction, we have illustrated the importance and popularity of Ti:Al_2O_3 as a gain medium for tunable and ultrashort lasers. Here, an explanation for the superior suitability of that material as a laser gain medium is given.

III.1.1 Physics of Vibronic Broadening

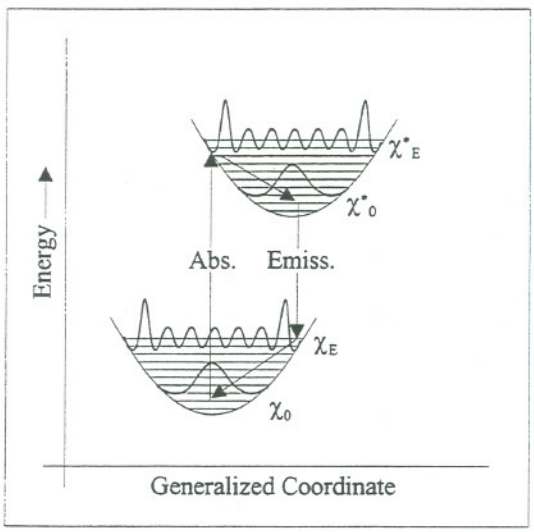

Figure III.1: Absorption and emission in a system with two vibronically broadened levels

A number of laser transitions in tunable lasers are based on *vibronical transitions*. The common feature of these transitions is the strong coupling between the laser active center (the Ti^{3+} ion in the case of Ti:Al_2O_3) and phonon modes of the host element. This makes the absorption and emission appear as broad bands. Since the phonon energy levels are discrete, one would expect the absorption to occur in a sequence of sharp lines. In reality, however, many secondary phonon modes of different frequencies are involved. This leads to bands which are smooth and featureless. It should also be noted that for a given photon energy, each center has an equal optical cross section. The broadening of the bands is therefore *homogeneous*.

Figure III.1 shows the general concept of lasing in such a system. For low temperature, absorption takes place mostly from the ground level χ_0 of the lower state. With increasing temperature, the higher levels become increasingly populated and can contribute to the absorption. Following optical excitation into χ_E^*, this mode quickly dissipates energy via phonon coupling to the bulk host. The system is then in the relaxed-exited state χ_0^*, which forms the upper laser level. After the stokes-shifted laser emission to χ_E, the system again relaxes quickly back to the ground state of the normal configuration.

As it can be seen from Fig. III.1, this sequence corresponds to an almost ideal four-level lasing configuration. Since for any finite pumping the populations between χ_0^* and χ_E are inverted, it is easy to obtain optical gain even for a low pumping power.

III.1.2 Linear Optical Properties of Ti:Sapphire

Sapphire as a Host Material

Sapphire (Al_2O_3) has a variety of properties which make it a desirable host material for optical applications. Probably the two most important ones are the high thermal conductivity and the wide transmittance window. The latter is twice as large as for a common optical BK7 glass and extends from below 200nm up 6μm. High thermal conductivity helps to maintain a uniform temperature distribution and reduces stress (Non-uniform thermal effects can limit the useful pump power, which is indeed a point of concern in laser amplifiers [68]). Other advantageous properties are the extreme surface hardness and the chemical inertness. Both make sapphire easy to handle.

Electronic Configuration

The electronic structure of a Ti^{3+} ion is a closed shell plus a single $3d$-electron [55]. The free-space, five-fold degeneracy of the energy levels is broken by the Jahn-Teller effect through a distortion of the crystal site. Lasing takes place between the two vibronically broadened ^2E_g and $^2T_{2g}$ states. Excited state absorption can be neglected, since higher energy states are too high to present a significant loss mechanism [10].

Transition Cross Sections, Gain and Loss

Important parameters for lasing materials are the stimulated emission cross section σ_e and the absorption cross section σ_a. Together with the population inversion density ΔN, they determine gain and loss coefficients[1]:

$$\begin{aligned} \gamma(\omega) &= \Delta N \sigma_e \\ \alpha(\omega) &= \Delta N \sigma_a. \end{aligned} \tag{III.1}$$

[1]Both coefficients are related to the *intensity* function, e.g., $I(z,\omega)=I(z=0,\omega)\exp\{\gamma(w)z - \alpha(w)z\}$.

To obtain short pulses, a large emission cross section is necessary for extracting energy efficiently. A small value of σ_e, on the other hand, has the advantage that a large inversion density can be obtained without the problems associated with amplified spontaneous emission (ASE). Ti:Al_2O_3 has a large value of σ_e=3-4 $\times$ 10^{-19}cm^2 for $E \perp$c-axis polarization [1, 55], which greatly facilitates energy extraction.

The broad fluorescence spectrum peaks at 800nm. It is featureless and drops under 10% of the peak value at 650nm and 1000nm. The absorbency of Ti:sapphire is centered around 500nm and extends from about 400nm to 600nm. Multiline Ar^+-ion lasers, as well as frequency doubled Nd:YAG and Nd:YLF lasers, are common pump sources. Relatively high absorption around 800nm presents the only disadvantage of Ti:Al_2O_3 . Losses on the order of 1-5%/cm at the lasing wavelength were reported for linear polarized light [46, 55]. Based on the evidence of post-growth annealing, it was suggested that Ti^{3+} in interstitial or defect sites cause the absorption [46]. Another explanation focuses on the influence of Ti^{3+}-Ti^{4+} ion pairs [36].

Energy Storage Time

A direct consequence of the large emission cross section and broad bandwidth is the short energy storage time (also: upper level- or inversion life time) T_1 of Ti:Al_2O_3 . At room temperature, T_1 equals (3.15$\pm$0.05)μs [55]. This explains the suitability of Ti:sapphire as a lasing material for the high-repetition rate regenerative amplifier: Since population inversion builds up with $\Delta N(t) \propto [1 - \exp(-t/T_1)]$ [73], any pumping for times longer than 1-2$\times T_1$ does no longer increase ΔN significantly. Efficient energy extraction in Ti:Al_2O_3 is therefore possible up to approximately 200kHz (e.g., 1.5$\times$ the inverse energy storage time).

III.2 Pulsed Laser Operation

Two techniques are used to obtain pulsed operation from a laser. In the first one, *Q-switching*, the loss of the cavity is modulated. This is usually achieved by means of electro-optic or acousto-optic modulators. While the quality factor Q of the cavity is lowered, a very large gain can build up. When Q is almost instantaneously restored to its original high value, the gain in the cavity is well above threshold. This causes the rapid build-up of

an intense pulse and in turn a fast depletion of the inversion. Q-switched pulses can be as short as a few nanoseconds.

Even shorter pulse durations are obtained by coupling the longitudinal modes of a resonator. Rather than having arbitrary phase relations, they are "locked" with respect to each other. Careful adjustment leads to constructive interference between the modes only during a very short time. This results in reliable generation of pulses as short as a few femtoseconds [4, 14, 18, 91]. Mode locking is explained at the end of this section.

Q-Switching

The theoretical treatment of Q-switching was presented in 1965 [40] and has remained essentially unchanged. It is based on a solution of the two *rate equations*, which describe the changes in population difference per volume $\Delta N(t)$ and photon density $n(t)$ in the laser. These important coupled differential equations are [73]:

$$\frac{dn}{dt} = K\Delta N n - \gamma_c n \tag{III.2}$$

$$\frac{d\Delta N}{dt} = R_p - \gamma_1 \Delta N - Kn\Delta N. \tag{III.3}$$

R_p is the pumping rate; $\gamma_1 \equiv 1/\mathrm{T}_1$ is the decay rate for the inverted population difference. K is a coupling coefficient between photons and lasing atoms (see [73]). The cavity decay rate γ_c describes the decay of the photon density in the resonator and is proportional to the overall losses in the cavity (including output coupling).

To solve (III.3) in the case of Q-switching, two simple assumptions can be made:

- The Q-switch opens instantaneously
- The build-up and the decay of the pulse take place on a timescale short compared to the inversion life time. Therefore, pumping and spontaneous emission can be neglected. Consequently, $R_p \equiv 0$ as well as $\gamma_1 \Delta N \equiv 0$.

With these simplifications, (III.3) yield:

$$\frac{dn(t)}{dt} = K\left[\Delta N(t) - \Delta N_{th}\right] n(t) \quad \text{and} \quad \frac{d\Delta N(t)}{dt} = -Kn(t)\Delta N(t). \tag{III.4}$$

$\Delta N_{th} \equiv \gamma_c/K$ is the population inversion at threshold. The two new rate equations can be solved only numerically and allow a reasonable description of experimental results [73].

The calculations show that the pulse shape for weak pumping is symmetric [84]. This changes for pump powers high above threshold: The pulse can build up rapidly, since the inversion and therefore the gain is large. The decay on the other hand approaches the cavity decay time $\tau_c \equiv 1/\gamma_c$. The reason is that the inversion is already depleted at the peak of the pulse, and the observed output is due to the free decay of photons in the resonator.

Relaxation Oscillations After the first, Q-switched pulse, the output power of the laser approaches its steady-state value in a series of sinusoidal *relaxation oscillations*. They take place on a timescale much longer than the cavity decay time or the duration of the initial, Q-switched pulse. The oscillations are caused by the coupling between photons–lasing atoms (III.3) and the finite gain recovery and cavity decay time.

Mode Locking

In a laser with a broad gain spectrum such as Ti:$Al_2 0_3$, the cavity emits in many longitudinal modes simultaneously. While the frequency spacing $\Omega = \pi c/l$ between two neighbouring modes is determined by the resonator length l, their relative phase is usually arbitrary. This causes the laser output intensity to fluctuate randomly around a mean value.

If, however, the longitudinal modes are all in phase, centered around a frequency ω_0, then the total amplitude for N modes can be summed up to the form:

$$\mathcal{E}(t) = \sum_{n=0}^{N-1} e^{i(\omega_0 + n\Omega)t} = \frac{e^{iN\Omega t} - 1}{e^{i\Omega t} - 1} e^{i\omega_0 t}. \tag{III.5}$$

(For simplicity, we assumed equal amplitudes for all modes). The intensity

is then given by

$$I(t) = |\mathcal{E}(t)|^2 = \frac{\sin^2(N\Omega t/2)}{\sin^2(\Omega t/2)}. \tag{III.6}$$

Some useful results can be readily obtained from this equation:

1. The laser emits a pulse train with a frequency $f_{rep} = \omega/2\pi = c/2l$.
2. The peak intensity is N^2 times that of a single mode
3. If we define a pulse width τ_0 as the time from the peak to the first zero, we get $\tau_0 = 2\pi/N\Omega$. Since $N\Omega$ is ultimately limited by the gain bandwidth $\Delta\omega_g$, we can estimate:

$$\tau_0 \sim \frac{2\pi}{\Delta\omega_g}. \tag{III.7}$$

This is simply the uncertainty principle. Ti:Al_2O_3 with its large $\Delta\omega_g \approx$ 400nm should therefore support pulse durations of 3-4fs.

Regardless of the particular kind of mode-locking technique, the idea to assure a fixed phase between different modes is always the same:

A device inside the laser cavity modulates the amplitude and/or the phase of the different longitudinal modes. The modes then "adjust" their phase in a way such that they experience minimum losses through the modulator. This is the case if the amplitude of the mode is maximal at the position of the modulator *and* at the time when the modulator losses are minimal. Provided that the modulation frequency equals the inverse cavity round trip time, the condition can be satisfied for each longitudinal mode; they are now "locked together".

Mode-locking is achieved with a large variety of different modulating devices. In *active mode-locking*, an externally driven acousto-optic modulator is used [26,74]. A technique which has been more successful in producing ultrashort pulses is *passive mode-locking* [16,19,57]. Here, a saturable absorber is placed inside the laser cavity. Among the initially random modes, the strongest ones bleach the absorber first, thus providing again a loss modulation with the cavity round trip frequency. Since the temporal response of the absorber is better than in the case of an externally driven element, shorter pulses can be obtained. The theory of passive modelocking was developed in a series of papers by Haus [27,28,30].

Phase Locking of Longitudinal Cavity Modes

Active Modelocking

cw - Lasers

- Lasing of different longitudinal modes is always present in the cavity
- Relative phase relation between modes is fixed through an active mode locker, which is driven with f_{ML}

Passive Modelocking

cw - Lasers

- A passive element (saturable absorber) is bleached with a frequency f_{ML} by the strongest initial wave packet. This causes all the other modes to lock to it

"Burst" Lasers

- For each pulse, lasing builds up from noise again.

Kerr Lens Mode Locking (KLM) Self mode-locking in Ti:Al_2O_3 is caused by the Kerr-effect. The Kerr effect is an intensity dependent modulation of the index of refraction:

$$n(I) = n_0 + n_2 I.$$

(n_0 is the low intensity index of refraction of the material and n_2 the intensity dependent Kerr coefficient.) After the first demonstration of a Kerr lens mode locked laser [78], several theories have been developed to describe how the Kerr effect locks the modes together [11, 29, 32, 56, 62]. All of them have in common that they propose a spatial mode at high intensity that is better matched to the gain region (or an additional aperture) than for lower intensities. The Kerr effect is used to explain the the spatial alteration of the TEM_{00} laser beam in Ti:Al_2O_3 [56]: The effect adds an intensity-dependent lens to the Ti:Al_2O_3 rod. Under low intensity cw- conditions, the laser crystal acts like a passive element. When short pulses are formed, the high intensity in the crystal causes the index of refraction to increase slightly. Subsequently, the beam comes to a tighter focus. A simple aperture inside the cavity can cause higher losses for the non-focused modes, thus forcing them into the low-loss operation.

Another contribution might arise from nonlinear coupling through $\chi^{(3)}$ [38]. This effect alone is strong enough to cause mode-locking only in the case of a long gain medium. However, it was shown that the effect should be included in the previously mentioned theory. Descriptions incorporating both the spatial beam alteration and nonlinear coupling produce more accurate

results [9].

It should finally be noted that KLM itself restricts to some extent the useful bandwidth of the gain medium and therefore will ultimately limit the shortest achievable pulse width [13].

III.3 Experimental Methods and Results

III.3.1 Crystal Characterization

Fig. III.2 shows the optical setup for the measurements. The Ti:sapphire crystal was pumped by a small frame argon laser; the probe beam was provided by a GaAlAs laser diode. Correct polarization of pump and probe beam was achieved with a $\lambda/2$ waveplate and a polarizing beamsplitter, respectively. A microscope objective focused the strongly diverging diode laser output. After passing through the crystal, pump- and probe beam were separated with a grating. We used a large area Ge-diode (to avoid influences of spot movement) and a lock-in amplifier for detection.

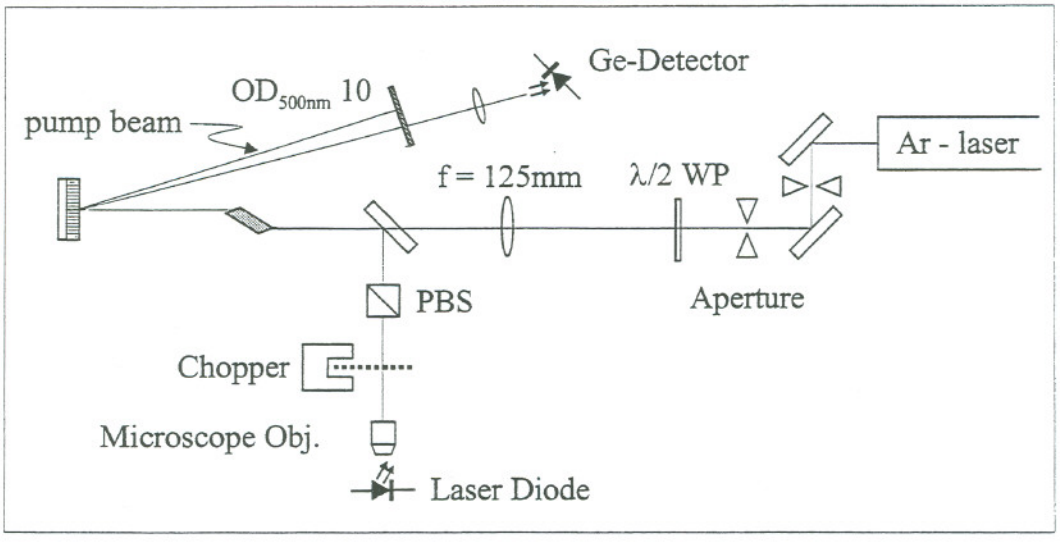

Figure III.2: Optical setup for crystal analysis

Ti:sapphire crystal The crystal was doped with 0.05 wt.% Ti_2O_3 in Al_2O_3. The rod had a diameter of 4mm and is 20mm long; it was Brewster-cut at both ends to minimize reflection losses. A beam entering the crystal at Brewster's angle propagates along the crystallographic c-axis. The long crystal and low doping are necessary to allow for sufficient heat dissipation over the absorption length of the crystal. To provide adequate cooling, the slab was mounted in a home-designed copper block, which was in turn connected

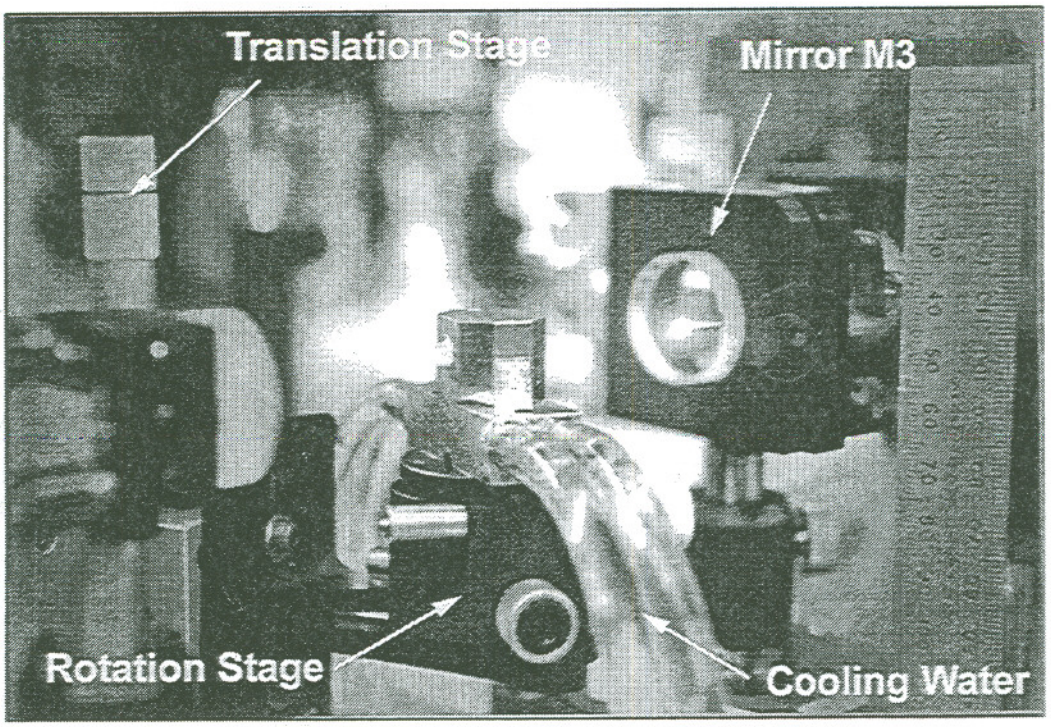

Figure III.3: Ti:sapphire crystal and mount (in final setup)

to a temperature-stabilized water chiller (T=15°C). Thermal grease assured good thermal contact between crystal and mount. A picture of the crystal in its mount is shown in Fig. III.3.

Argon Laser For these temporary measurements, a small frame argon-ion laser pumped the crystal. The laser emitted up to 9.5W of "multiline visible", e.g., with an intensity ratio of 5:1 between 514nm and 488nm lines. Unless noted otherwise, TEM_{00} operation was used.

GaAlAs Laser Diode A GaAlAs laser diode emitted up to 4mW in a single line at 821nm. The output diverged strongly and had a highly inhomogeneous transverse mode profile. To avoid both frequency and power fluctuations, the diode was mounted on a heat sink with a thermoelectric cooler.

Results and Discussion

Index of Refraction: The index of refraction and the correct cut of the rod were verified. For that purpose, the pump beam was incrementally rotated by an angle ϑ from p- to s-polarization. Using Fresnel's equations, it can be shown that the transmission varies with:

$$\mathrm{T}_n = \cos^2\vartheta + \tau^2 \sin^2\vartheta, \text{ where } \quad \tau = \frac{4n^2}{(1+n^2)^2} \,. \tag{III.8}$$

The transmission T_n is normalized to p-polarization, and the absorption is assumed to be independent of ϑ. A departure from the latter assumption, as well as unprecise cutting, would result in a poor fit. However, measurements showed an excellent agreement with (III.8). From the best-fit for τ, a value of $n = 1.76$ was calculated This agrees with the literature [55].

Absorption Coefficients: The absorption was determined at both the pump and the lasing wavelength. At 820nm, it was found that our crystal absorbs $(2.2 \pm 0.5)\% \times \mathrm{cm}^{-1}$. This number is well within the range mentioned in (III.1.2). For the pump beam, we measured an absorption coefficient of $\alpha_{pump} = (1.70 \pm 0.02) \times \mathrm{cm}^{-1}$, using 100mW of power focused into the crystal. At the operating power of the regenerative amplifier, the coefficient dropped slightly due to absorption saturation. In any case, more than 96% of the pump energy were absorbed in the 20mm long Ti:Al_2O_3 rod.

Gain Measurements: Results of the single pass gain[2] measurements are shown in Fig. III.4. (a) indicates a linear dependence between pump power and gain. According to (III.1), the gain varies in first approximation linearly with ΔN, which in turn is proportional to the absorbed power per volume. Extrapolation of the graph towards P_{pump}=0 again illustrates the rather high absorption of the crystal. The value obtained by a linear regression agrees with the preceeding measurement of α.

The graph already allows us to get an idea about the lasing threshold of a laser built with this crystal. To establish positive feedback, the cavity gain has to exceed the losses. Assuming no other losse than an additional 3% output coupler, we would expect lasing to start at about 2.5W.

[2]With "gain", we refer to the gain in the crystal, e.g., $g = I(z,\omega)/I(z=0,\omega) = \exp\{\gamma(w)z - \alpha(w)z\}$. $g < 1$ indicates an overall loss in the crystal.

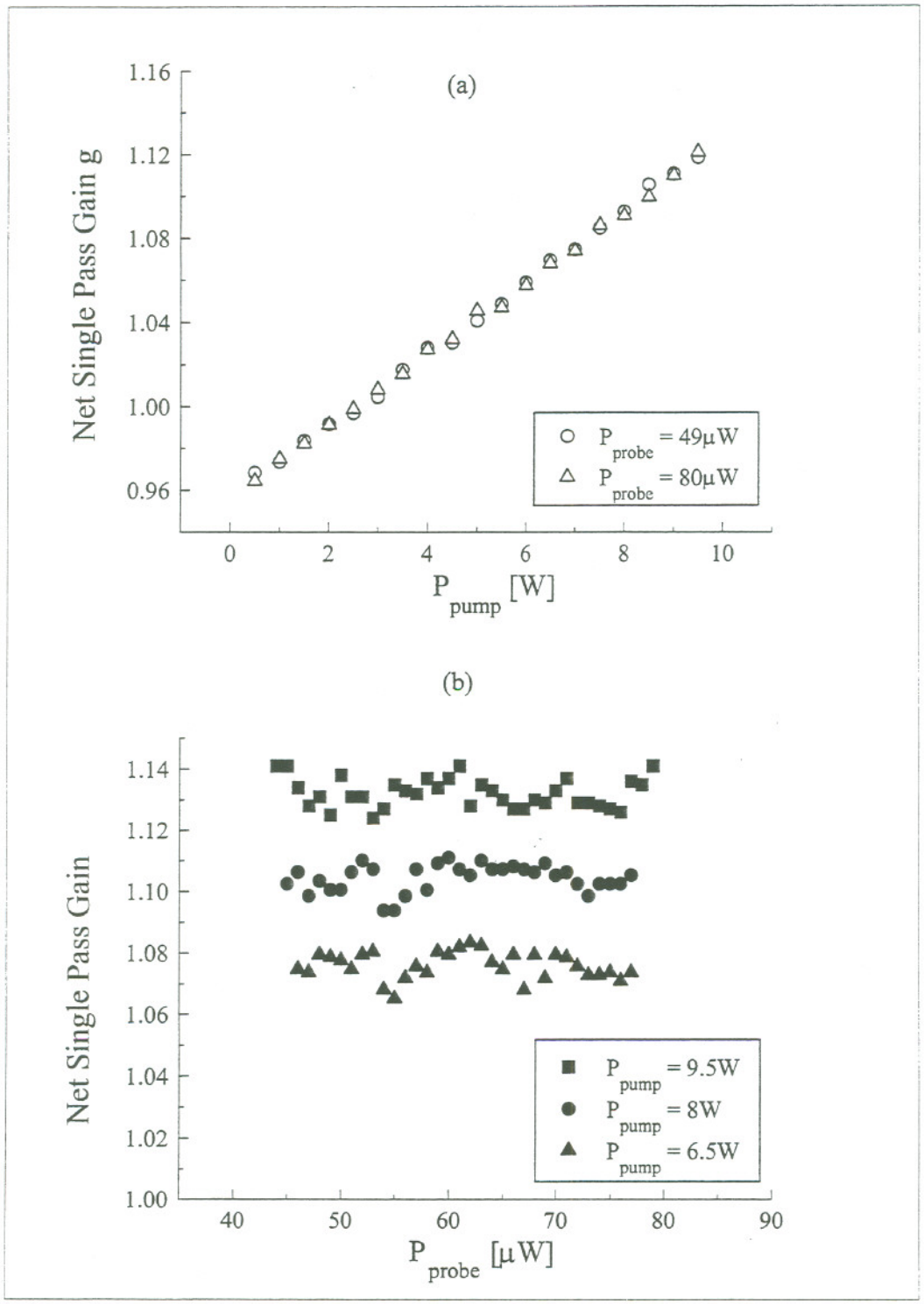

Figure III.4: Net single pass gain in the Ti:sapphire rod

Fig. III.4 (b) confirms the values for g from (a), and shows that for low power the gain is independent of the injected power. For much higher P_{probe}, saturation of the gain would occur. This, however, is not a concern if only probe powers of tens of microwatts are used.

Emission Cross Section: From the gain measurement, we can now estimate the emission cross section of the Ti^{3+} ions in sapphire at 820nm. Experimentally, σ_e can be obtained by measuring the gain of a TEM_{00} probe beam which propagates collinear with the pump beam. If the pump beam, too, is in TEM_{00}-mode, the emission cross section is given by [55]:

$$\sigma_e = \frac{\pi^2 (b^2+1) \hbar c w_{pu}^2 g}{\lambda_{pu} P_{pu} \mathrm{T}_1 [1 - \exp(-\alpha_{pu} l)]}. \tag{III.9}$$

(T_1 = fluorescence lifetime, g = measured fractional gain in the probe beam, α_{pu} = absorption coefficient of the pump beam, l = crystal length, λ_{pu} = pump wavelength, P_{pu} = pump power at the crystal entrance surface, b = ratio between the probe beam radius and the radius of the pump beam w_{pu})

With the laser beam propagation laws, we can estimate w_{pu} to $\approx 100\mu$m. b is approximately unity. In surprisingly good agreement with the literature [55], we get

$$\boxed{\sigma_e = 3 - 4 \times 10^{-19} \mathrm{cm}^{-2}.}$$

Influence of Pump Mode Structure: Fig. III.5 plots the gain vs. the mode of the pump beam. The need for a good TEM_{00} mode is clearly illustrated. For TEM_{00} operation, the aperture can be changed without too much influence on the gain. A drop can be observed while changing to multimode operation. The transition between multimode and TEM_{00} operation of the laser is in reality rather smooth— a fact which is reflected by Fig. III.5.

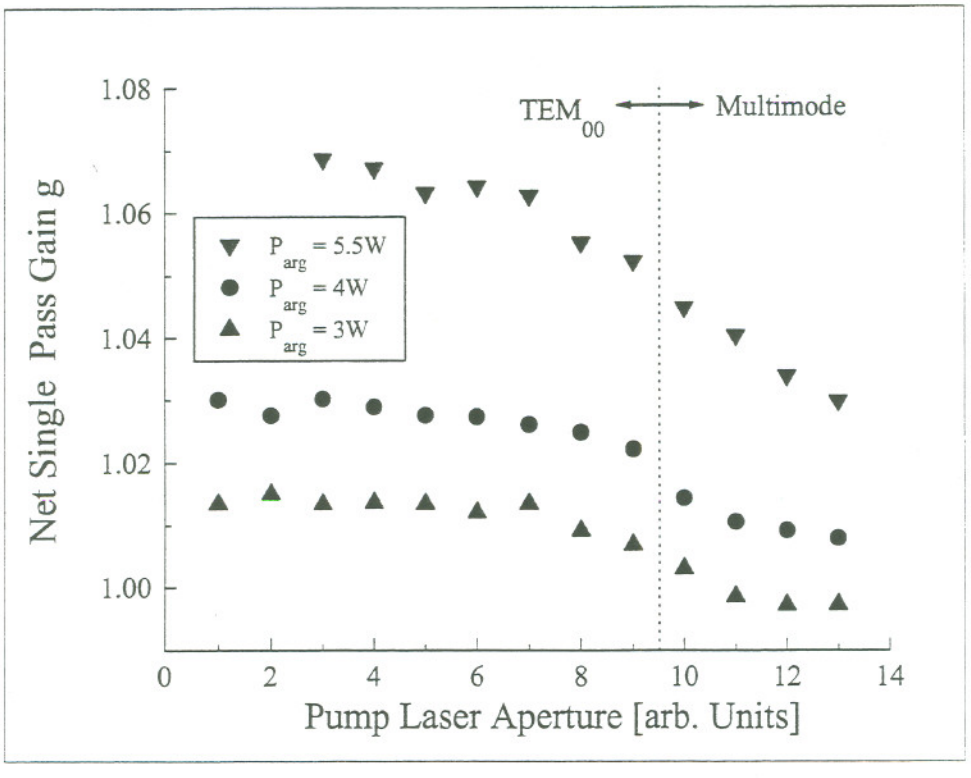

Figure III.5: Dependence of the net single pass gain on the transversal mode structure of the bump beam. Smaller numbers indicate a smaller aperture.

III.3.2 Laser Operation of the Cavity

Measurements of the cavity laser parameters were carried out with the setup shown in Fig. III.6. Since no switching of pulses into and out of the cavity was necessary, the cavity dumper was replaced by a 3.5% output coupler. The cavity was astigmatically compensated (as described in Chapter 3). The output coupler and M5 were flat mirrors, M3 and M4 had a radius of curvature of 0.1m. All mirrors are single stack, broadband coated with a maximum reflectivity at 820nm. M3 in addition is highly transmitive at the pump laser wavelength. L1 is a plano-convex lens with a focal length of 132mm at 500nm. To monitor the average output power, we used a silicon-based power meter (PM), calibrated for 820nm. For pulsed operation, we detected the leakage through one of the high reflectors with a fast silicon photodiode (risetime $\sim$ 1ns).

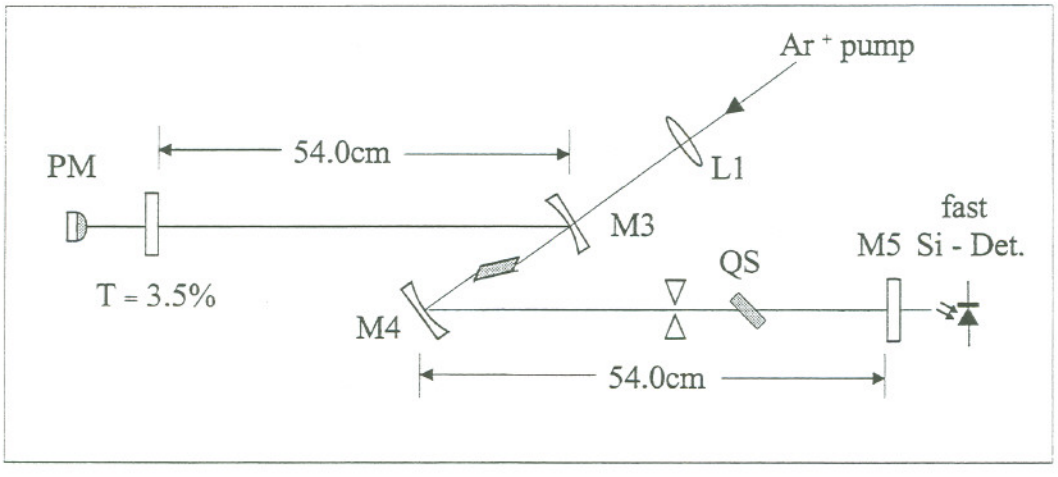

Figure III.6: Experimental setup used for measuring the cw- and pulsed operation of the cavity. The distance between crystal surface and M3, M4 is 47mm; L1 has a focal length of 132mm at 500nm

Results and Discussion

Laser in cw Operation The following table summarizes the experimental results with the free running cavity and compares them to theoretical predictions:

Parameter	Experiment	Theory
Lasing Threshold	(2.25±0.5)W	(2.5±0.5)W
Max. Output Power (9W Pump)	1W	N/A
Beam Divergence	1.0mrad	0.92mrad
horiz. beam radius at O.C.	3.1×10^{-4}m	2.9×10^{-4}m
vert. beam radius at O.C.	3.6×10^{-4}m	2.9×10^{-4}m

The theoretical values for beam divergence and radius were taken from the theoretical cavity simulations in chapter I, and the threshold can be directly derived from the gain measurements.

Without exception, the beam parameters are in good agreement with those predicted by theoretical cavity simulations and preliminary experiments.

Q-Switched Laser Operation A typical Q-switched laser output pulse is shown in Fig. III.7: After the initial spike, relaxation oscillations eventually lead to the equilibrium value of the output. Closing the Q-switch causes the intensity to drop again. The influence of different pump powers on the pulse shape is illustrated in the inset. As predicted in (III.2), it becomes increasingly asymmetric with higher powers.

Relaxation Oscillation: It can be shown [73] that the frequency of the oscillation following the initial spike is given by

$$\omega_{relax} = \sqrt{(r-1)\,\gamma_1\gamma_c}\ , \text{ where } \quad r \equiv P_{pump}/P_{pump}^{threshold}.$$

With 6W pump power, an inversion decay rate of γ_1=0.3×10^6s^{-1} (obtained from [55]) and a cavity decay rate γ_c=$(15\pm1)\times10^6$s^{-1}, a relaxation oscillation frequency of ω_{relax}=2.7×10^6s^{-1} is expected. From the data of Fig. III.7, we get in fair agreement with the theory.

$$\omega_{relax}^{exp} = (2.3 \pm 0.2) \times 10^6\text{s}^{-1}.$$

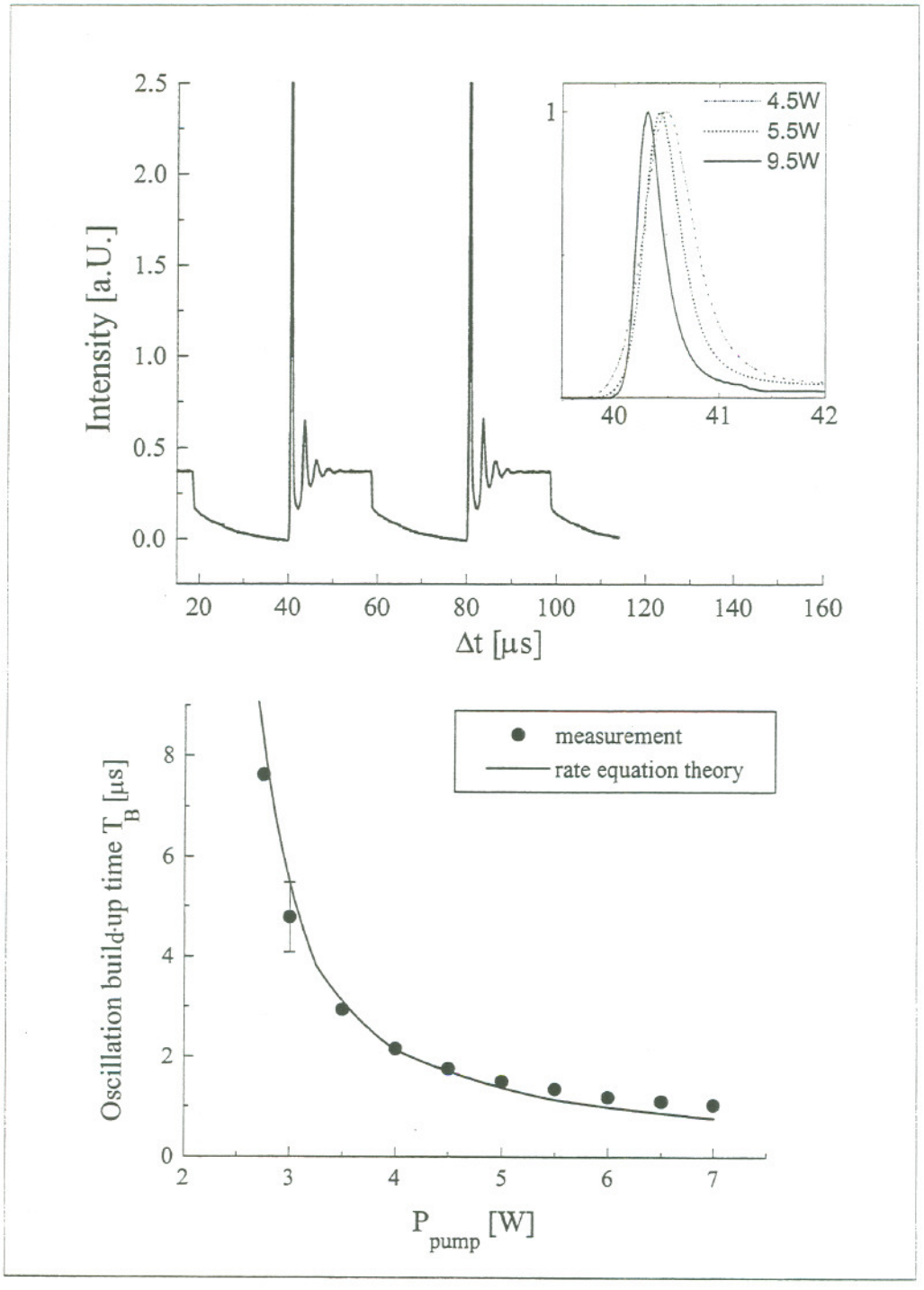

Figure III.7: **Top:**Q-switched pulse train as monitored through M5. The Q-switch is opened $\approx 1\mu s$ before the initial spike builds up. The inlay shows the different shapes of the Q-switched pulse for different pump powers on a normalized scale. **Bottom:** Delay in buildup of a Q-switched pulse vs. pump power.

Pulse Build-Up Delay: We mentioned in (III.2) that stronger pumping results in a faster build-up of the Q-switched pulse. The bottom graph of Fig. III.7 reflects that fact. From (III.4), the theoretical oscillation build-up time T_B can be derived [73]:

$$T_b = \frac{25 \pm 5}{r - 1} \times \gamma_c^{-1} \tag{III.10}$$

(The 20% margin in the numerator reflects an uncertainty in the initial photon density in the cavity.) The theoretical graph shows good agreement with the data points.

Repetitive Q-switching Fig. III.8 plots average power and peak energy in the case of repetitive Q-switching. As long as the time between two successive

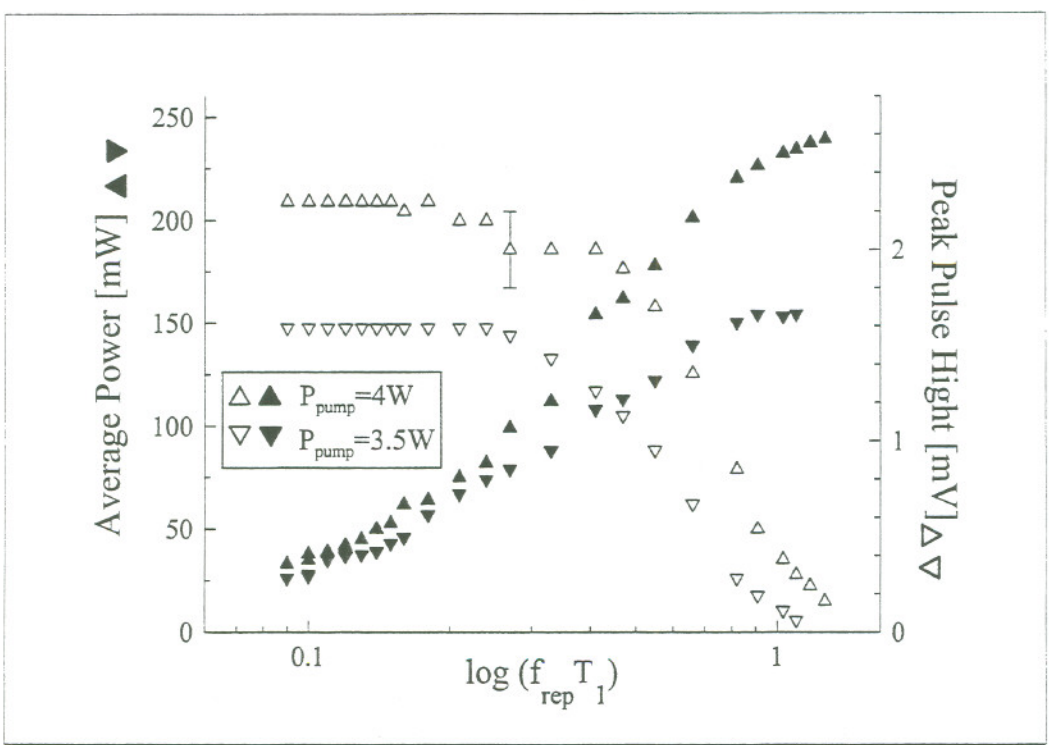

Figure III.8: Average power (solid triangles) and energy per pulse (unfilled triangles) for repetitive q-switching

pulses is long enough to allow for complete gain recovery, the energy per

pulse remains constant. As a result, the average power increases linear with the repetition rate. At faster repetition rates, on the other hand, the average power is expected to approach the cw- value, whereas the energy per pulse decreases.

Mode-Locking As mentioned above, a delicate balance of parameters is necessary to obtain stable mode-locking from a laser cavity. In our case, no further attempt was made to optimize the cavity for short pulsed operations. Nevertheless, the cavity could be operated mode-locked for as long as 15min, as shown in Fig. III.9.

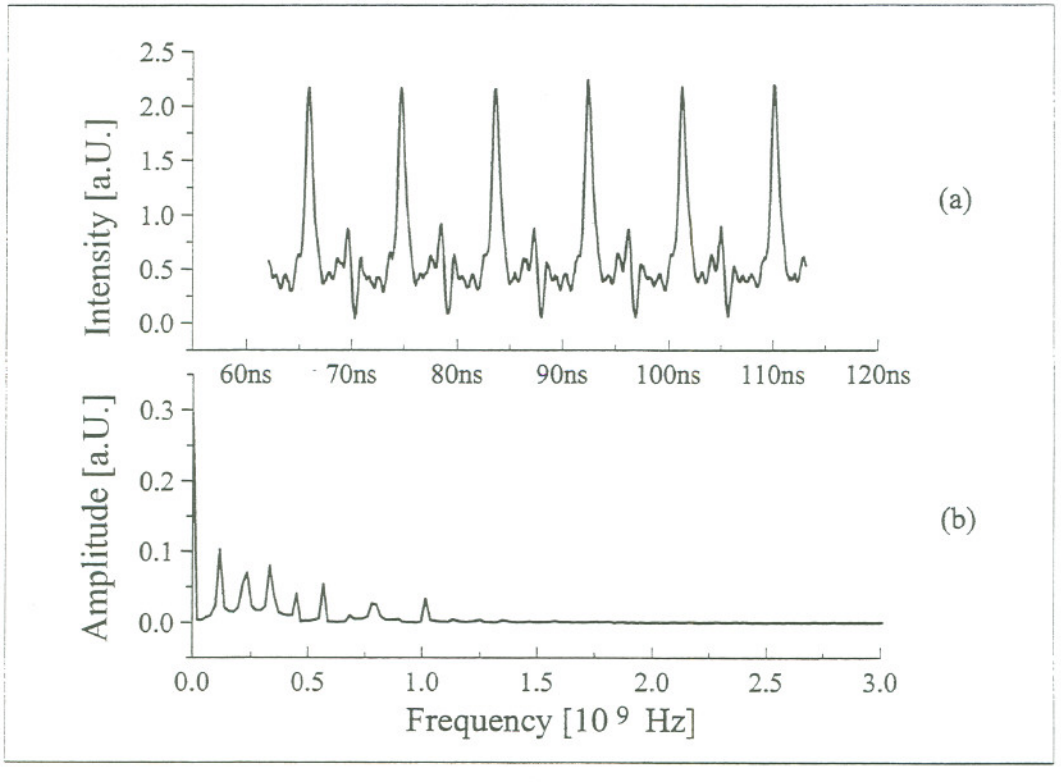

Figure III.9: The mode-locked pulse train as monitored through the mirror M5 is shown in (a). (b) shows the spectrum as derived by fast fourier transformation. In both cases, the resolution is limited by the instrument response of $\approx$ 1ns or 1×10^9Hz, respectively

Cavity Length: Since the spacing between two pulses is given by the inverse repetition rate $1/f_{rep} = c/2l$, a very accurate determination of the

cavity length is possible. From f_{rep} =127.2MHz, we obtained a total length l=1.174m for the simple cavity in Fig III.6. Mode locking (although less stable) was also possible in the final cavity. Here, f_{rep} =113.2MHz yielded l=1.325m.

Pulse Duration: The long rise time (1ns) of the photodoide does not allow to give a number for the pulse length. Since the cavity was not entirely stable, no autocorrelation measurement was performed.

Fourier Analysis and Pulse Shape: Even though the frequency analysis is again limited by the temporal response of the diode, we can verify the existence of several longitudinal cavity modes, spaced by f_{rep}. Their different amplitudes cause the intensity fluctuations between the main pulses.

Master Oscillator As a master oscillator for our amplifier, we used the Clark-MXR NJA-4 Ti:sapphire laser kit. The laser is typically pumped with 4W from a multiline argon laser. Two intracavity prisms provide dispersion compensation. Pulses as short as 30fs can be obtained after additional external compression. However, a more stable operation is possible with 100fs pulses. The repetition rate of the laser is 103MHz. The output spectrum and the autocorrelation trace for the uncompressed 30fs operation are shown in Fig. III.10. For 100fs pulses, the center of th emission spectrum shifted towards 840nm.

Since the pulse in (b) was not recompressed, it is not transform limited. This fact is reflected by the time-bandwidth product of 1.41, indicating uncompensated dispersion (The issue of pulse compression and dispersion is described in an own chapter).

A major drawback of the laser is the unstable operation, both on short and long timescales. We believe that the cause for long term ($\sim$ hrs) instabilities are temperature fluctuations in the laboratory. Measurements showed changes of as much as 6°C within 12hrs. Intensity changes from pulse to pulse are partially caused by air currents and fluctuations of the pump beam. Complete enclosure of the entire beampath increased the stability.

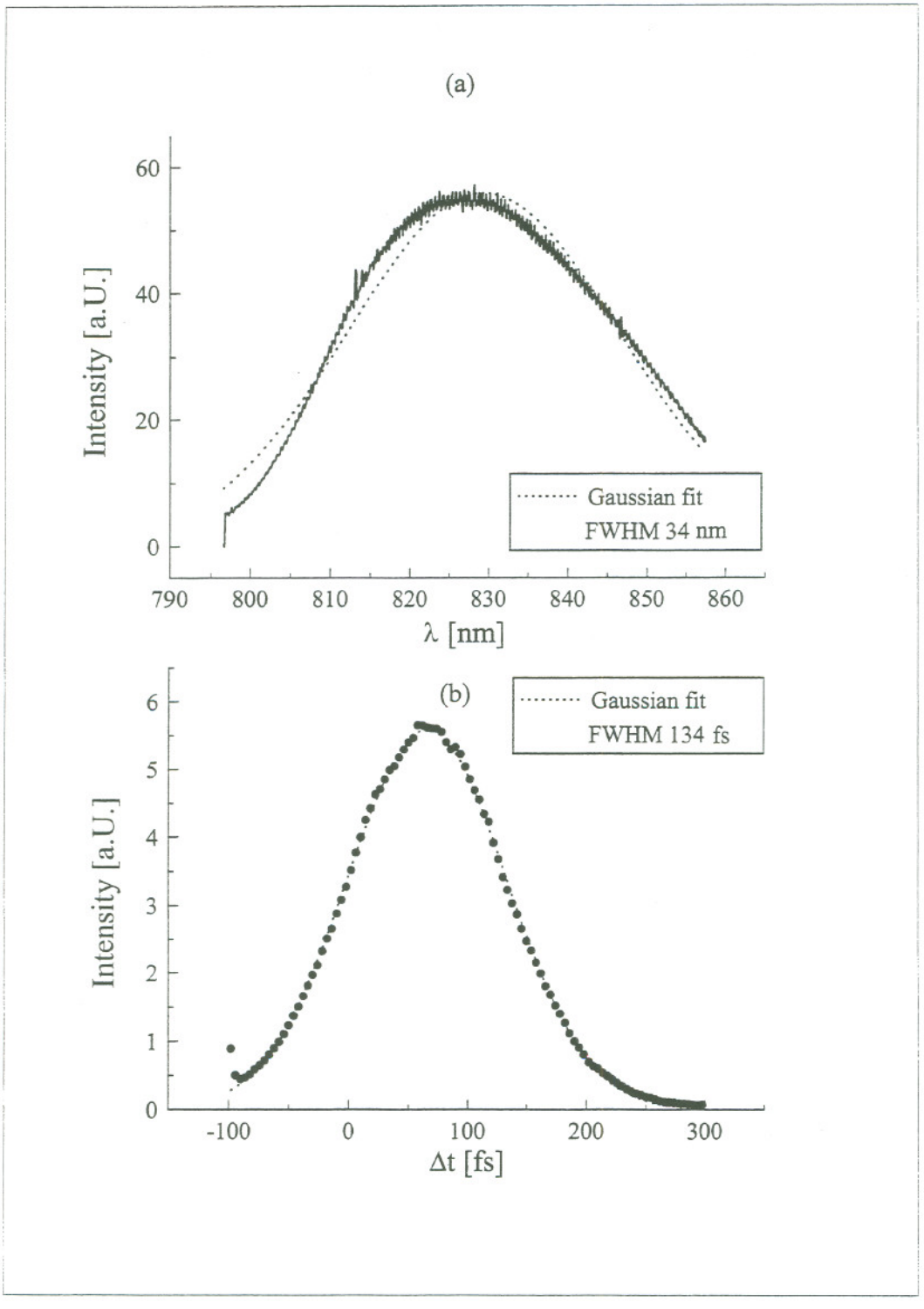

Figure III.10: Output spectrum (a) and autocorrelation trace (b) of the master oscillator

Chapter IV

Pulse Shaping

One of the most important issues in generation and manipulation of ultrashort pulses is the control of dispersion. This is not only necessary to avoid temporal and spectral distortion. To obtain sub-100fs pulses from a laser system, a careful balance between different dispersion mechanisms is required.

In our regenerative amplifier, a stretcher-compressor combination is needed for two reasons:

- Prior to injecting pulses into the amplifier, a stretcher must be used to increase the pulsewidth. This is necessary to avoid nonlinear optical effects and material damage.

- After the amplification, a compressor not only compensates for the effect of the stretcher, but also for the dispersion due to several passes inside the amplifier resonator.

The first section of this chapter introduces some of the ideas of pulse propagation in a linear medium. They are then applied towards the theory of optical pulse stretching and compression.

We developed a stretcher/compressor combination for the regenerative amplifier. The setup is described in the second part. Theoretical simulations and experiments to evaluate the performance are described.

IV.1 Introduction and Theoretical Background

The terms of importance for the discussion of pulse stretching and compression are introduced in this chapter. The principles, however, are valid not only for the deliberate shaping of ultrashort optical pulses. They apply for any signal which propagates in a linear dispersive medium.

IV.1.1 Chirped Pulses

For a fixed spatial position, a Gaussian pulse[1] with carrier frequency ω_0 can be expressed as:

$$E(t) = \exp\left(-at^2\right) \times \exp\left\{i\left(\omega_0 t + bt^2\right)\right\} \equiv \exp\left(-\Gamma t^2\right) \times \exp\left\{i\omega_0 t\right\}. \tag{IV.1}$$

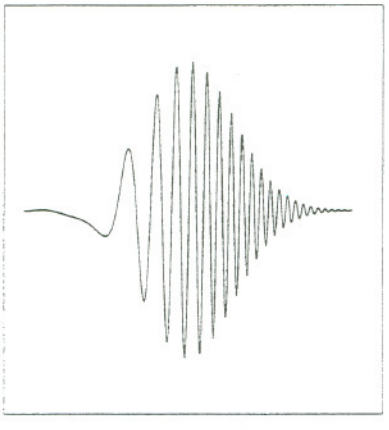

Figure IV.1: Linearly chirped pulse with Gaussian envelope function

The *Complex Gaussian Parameter* is defined as $\Gamma = a - ib$ [73]. Using the FWHM definition, the intensity envelope has a width of

$$\tau = \sqrt{\frac{2\ln 2}{a}}. \tag{IV.2}$$

The total phase of the pulse is given by $\phi_{tot} = \omega_0 t + bt^2$. From that, the instantaneous frequency of the pulse can be derived as:

$$\omega_i = \frac{d\phi_{tot}}{dt} = \omega_0 + 2bt \tag{IV.3}$$

If the parameter b is nonzero, the frequency varies linearly with time. Such a signal is called *chirped*. By definition, a pulse has a positive chirp if the lower frequencies can be found at the leading edge of the pulse. The parameter b serves as a measure of how strong the chirp is. Fig IV.1 shows a (rather strongly) chirped pulse with a Gaussian envelope function.

[1] The mathematical treatment is somewhat simplified if a Gaussian pulse is chosen. This shape also fits our pulses best. It should be nevertheless noted that pulses of any given shape undergo the same transformations

IV.1.2 Time-Bandwith Product

The Fourier-transformation of the Gaussian pulse in time (IV.1) leads to a spectrum of the same shape:

$$E(t) = \exp\left(-\Gamma t^2 + i\omega_0\right) \Longleftrightarrow \tilde{E}(\omega) = \exp\left[-\frac{(\omega-\omega_0)^2}{4\Gamma}\right] \tag{IV.4}$$

The FWHM of the power spectrum $\left|\tilde{E}(\omega)\right|^2$ is the spectral width $\Delta\omega_p$ (in rad/sec) of the pulse. Dividing by 2π yields the *bandwidth* of the signal in Hz:

$$\Delta f_p \equiv \frac{\Delta\omega_p}{2\pi} = \frac{\sqrt{2\ln 2}}{\pi}\sqrt{a\left[1+(b/a)^2\right]} \tag{IV.5}$$

Equation (IV.5) illustrates that for a signal with fixed temporal width (determined by the parameter a) the bandwidth increases if the pulse is chirped. The smallest spectral width on the other hand is obtained for an unchirped pulse. It is straightforward to define a *time-bandwidth product* (TBP)

$$\tau_p \Delta f_p = \left(\frac{2\ln 2}{\pi}\right) \times \sqrt{1+(b/a)^2} \approx 0.441 \times \sqrt{1+(b/a)^2}. \tag{IV.6}$$

The minimum value of the TBP for an unchirped Gaussian pulse therefore equals 0.441. Equation (IV.6) is only a special case of the Fourier theorem which constrains the TBP of any pulse by the uncertainty principle $\Delta f_{rms}\Delta\tau_{rms} \geq 1/2$. The exact value of $\tau_p\Delta f_p$ depends one various factors, such as

- the exact shape of the signal,
- how "width" is defined (FWHM, rms, etc.),
- whether the pulse has a substructure, such as chirp.

Once the shape and definition of the width are known, the value of the TBP gives information about the structure of the signal. Pulses with a value of $\tau_p\Delta f_p \approx 0.5$ have little or no frequency variation within their envelope function. Those signals are called *transform limited*. The following table summarizes the TBP values for some common functions:

Function	I(t)	τ_p/τ_{ac}	$\Delta f_p \times \tau_p$
Square	$I(t) = \begin{cases} 1 & \text{for } \lvert t\rvert \le \tau_p/2, \\ 0 & \text{for } \lvert t\rvert > \tau_p/2 \end{cases}$	1	1
Gaussian	$I(t) = \exp\left(-\frac{4(\ln 2)t^2}{\tau_p^2}\right)$	0.707	0.441
Hyp. Secant	$I(t) = \mathrm{sech}^2\left(\frac{1.76t}{\tau_p}\right)$	0.648	0.315
Lorenzian	$I(t) = \left[1 + 4t^2\tau_p^{-2}\right]^{-1}$	0.5	0.221

τ_{ac} $\equiv$ FWHM of autocorrelation function
τ_p $\equiv$ FWHM of intensity envelope
Δf_p $\equiv$ FWHM of power spectrum

IV.1.3 Pulse Propagation in a Dispersive Media

In free space, the propagation constant k has a linear dependence on the frequency: $k = \omega/c_0$. In general, k might be a more complicated function of ω. If only a narrow frequency range is of interest, the propagation constant[2] can be expanded into a power series around a center ω_0:

$$\begin{aligned}\phi(\omega, z) =& \phi(\omega_0, z) + \left(\frac{d\phi}{d\omega}\right)_{\omega_0} \times (\omega - \omega_0) + \frac{1}{2}\left(\frac{d^2\phi}{d\omega^2}\right)_{\omega_0} \times (\omega - \omega_0)^2 \\ &+ \frac{1}{6}\left(\frac{d^3\phi}{d\omega^3}\right)_{\omega_0} \times (\omega - \omega_0)^3 + O(\omega - \omega_0)^4 \end{aligned} \tag{IV.7}$$

To interpret the different terms in (IV.7), we assume a Gaussian pulse (IV.1) with parameters ω_0, Γ_0. It can be shown [73] that after propagating a distance z in a media with a dispersion relation (IV.7) the pulse takes the form:

$$E(z,t) = \exp\left[i(\omega_0 t - \phi(\omega_0, z)\right] \times \exp\left[-\Gamma(z) \times (t - \phi'(\omega_0, z))^2\right] \tag{IV.8}$$

with $1/\Gamma(z) = 1/\Gamma_0 - 2i\phi''$.

[2] It is customary not to expand k, but rather the total phase shift $\phi(\omega, z) = k(w)z$. The linear z-dependence of ϕ is often not explicitly written out.

Phase Velocity: The first term on the left hand side shows that the phase of the carrier frequency appears to be delayed by $t_\phi = \phi/\omega_0$. As a result, the sinusoidal waves within the pulse envelope will have moved forward with the *phase velocity*

$$v_\phi = \frac{z\omega_0}{\phi(\omega_0, z)} = \frac{\omega_0}{k(\omega_0)} \tag{IV.9}$$

Group Velocity: In the same way, the second term of (IV.8) determines the speed with which the Gaussian envelope moves forward. With the *group delay* $t_g = \phi'$, the *group velocity* calculates to

$$v_g = \frac{z}{\phi'} = z \left(\frac{d\omega}{d\phi}\right)_{\omega_0} = \left(\frac{d\omega}{dk}\right)_{\omega_0}. \tag{IV.10}$$

Group Velocity Dispersion: The second derivative of the phase acts as a dispersion term for the group velocity; it now depends on the frequency:

$$\frac{d^2\phi}{d\omega^2} = \frac{d}{d\omega}\left(\frac{d\phi}{d\omega}\right) = \frac{d}{d\omega} t_g \tag{IV.11}$$

It is this part of the power series (IV.7) which is primarily responsible for signal stretching and compression. If a pulse with different frequency components experiences group-velocity dispersion (GVD), these components are delayed or advanced with respect to each other. Consequently, their spatial position also changes, thus altering the spatial shape of the pulse. As a result, the signal obtains a linear chirp.

Third- and Higher Order Dispersion To shape optical pulses shorter than 100fs, the higher-order terms of (IV.7) become increasingly important [18, 47]. If they are included, the group delay no longer varies linearly with frequency.

IV.2 Pulse Compression and Stretching

It has been shown in the last section how second-order or group velocity dispersion can change the temporal shape of a signal. This section deals with the technical realization to control dispersion.

Dispersion can be found in all optical media. Most common materials exhibit positive second-order dispersion in the visible region, turning into negative values in the near infrared. Since even the dispersion in air can broaden a very short optical pulse, tunable devices which compensate for both positive and negative GVD are needed. If the systems are linear, the order in which the dispersion is introduced does not matter.

The two most widely used techniques for optical pulse manipulation are Prisms [18, 20, 54] and gratings [18, 47, 53, 81]. While the latter ones present the advantage of causing much ($\approx \times 10^2$) higher GVD, prisms have a better optical efficiency. This makes them the preferred choice inside laser cavities, where insertion losses are crucial. However, the general principle is in both cases the same: Frequency dependent differences in diffraction result in different optical paths.

IV.2.1 Grating Compressor

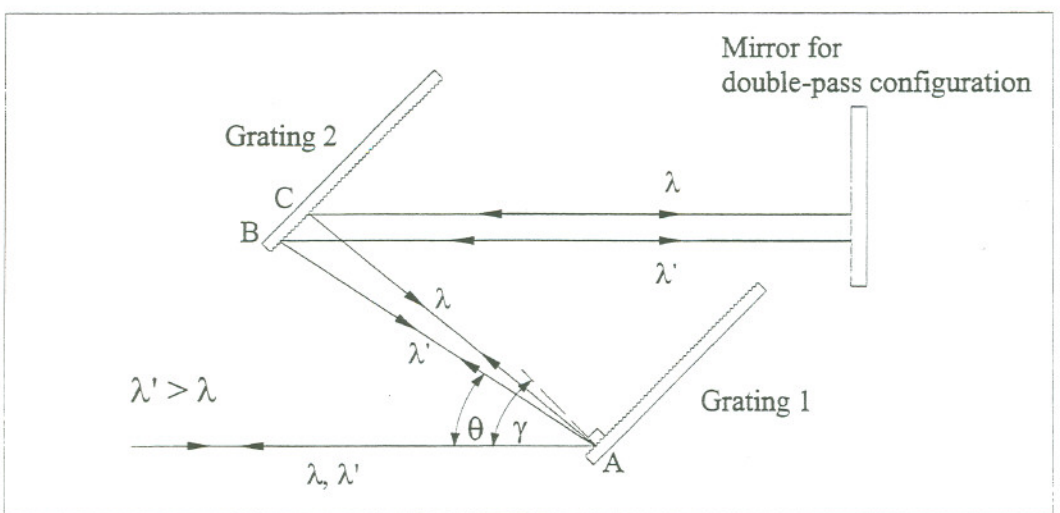

Figure IV.2: Geometrical arrangement of a pulse compressor using diffraction gratings. γ is the angle of incidence and θ the acute angle between incident and diffracted rays. Grating 1 and 2 are identical and parallel with a grating constant d. The wavelength dependent slant distance $\overline{AB}$ is b.

Fig IV.2 illustrates the principle of a two-grating optical pulse compressor. It uses the wavelength dependent dispersion of the gratings to introduce a group delay t_g which increases in a first approximation linearly with frequency.

The first of the two parallel gratings diffracts the incoming beam. The angle θ is larger for longer wavelengths. After the second grating, the rays are again parallel, but with the lower frequencies having traveled a longer optical path. This corresponds to a positive GVD. However, after the first pass, different frequency components are spatially separated. By passing the system a second time in reverse direction, the spatial effect is compensated, while the dispersion is doubled.

The first analytical expression for the phase change in a grating compressor was given by E. B. Treacy [81]:

$$\phi = \phi_0 + \kappa(\omega - \omega_0) - \frac{(\omega - \omega_0)^2}{2\mu} + \frac{1}{6}\sigma(\omega - \omega_0)^3 \tag{IV.12}$$

The expansion coefficients κ, μ and σ are given as:

$$\begin{aligned} \kappa &= bc^{-1}(1 + \cos\theta) \\ \mu^{-1} &= \frac{4\pi^2 bc}{\omega_0^3 d^2 \left\{1 - [(2\pi c/\omega_0 d) - \sin\gamma]^2\right\}} \\ \sigma &= 3(\pi\omega_0\mu)^{-1}\left(1 + \frac{\lambda}{d}\sin\gamma + \sin^2\gamma\right) \end{aligned} \tag{IV.13}$$

Here, b is the slant distance $\overline{AB}$, d the grating constant, γ the angle of incidence. θ is the acute angle between incident and diffracted rays and c the speed of light. Both grating separation b and angle of incidence γ are used to adjust the compressor. In practice, first the distance between the gratings is chosen to eliminate GVD. Then, adjustments of the angle of incidence minimize third-order effects. Eq. (IV.12) does not take into account effects such as Gaussian beams, a finite spot size or deviations from the paraxial approximation. To obtain more accurate results, ray-tracing computer simulations are commonly used [47].

IV.2.2 Grating Stretcher

With only slight modification, a pulse compressor can be used as a stretcher. O. E. Martinez pointed out that this is in fact true for any dispersive device which relies on spatial separation between its components [54]. Fig IV.3 shows how by placing a 1 : 1 telescope in between them, the effective distance can be made negative. With a "negative" grating separation, the expansion

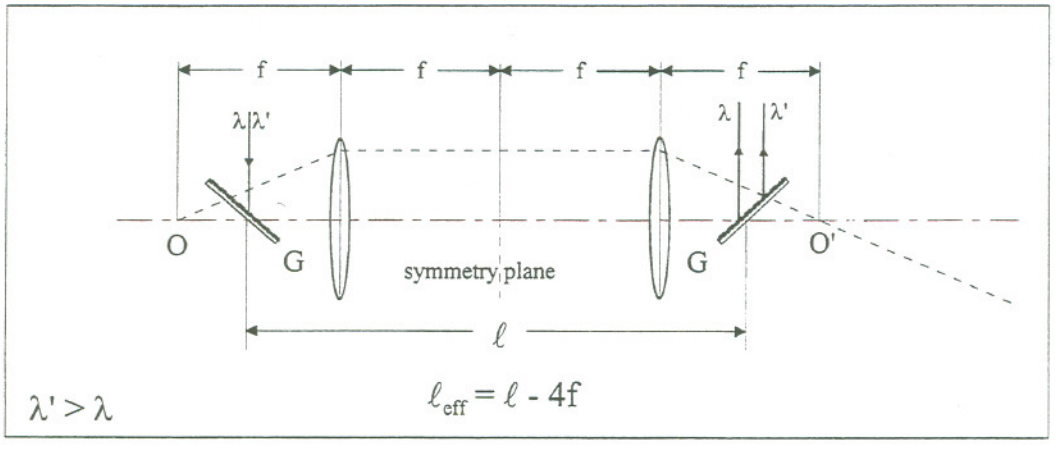

Figure IV.3: Effect of a 1 : 1 telescope in a grating stretcher: The distance between O and O' (focal points) must be subtracted from l, because the optical paths for propagation at different angles are identical. If the gratings G are located inside the focal planes, the effective distance between the gratings is negative. The beams λ and λ' are shown schematically

coefficients (IV.13) change their sign, which results in a negative GVD. A more detailed derivation, which takes into account finite spot sizes, can be found in [53].

The design of Fig IV.3 can be slightly improved if reflective instead of transmitive optics are used [66]. This avoids lens aberrations. Furthermore, by exploiting the symmetry properties of Fig IV.3, a more compact setup is possible. In this case, only one grating and one focusing element are necessary; a flat mirror placed in the symmetry plane "replaces" the second grating [47, 90].

Fig IV.4 summarizes the two possibilities of pulse shaping by second order dispersion. Once pulse is chirped, it can be broadened in time by positive GVD. In first approximation, the delay is linear in frequency (solid line). Higher order effects cause derivations (dashed line). By introducing a device with negative GVD, a broad, chirped signal can be compressed. Due to the different propagation times, frequency components can "catch up", e.g. form a short pulse.

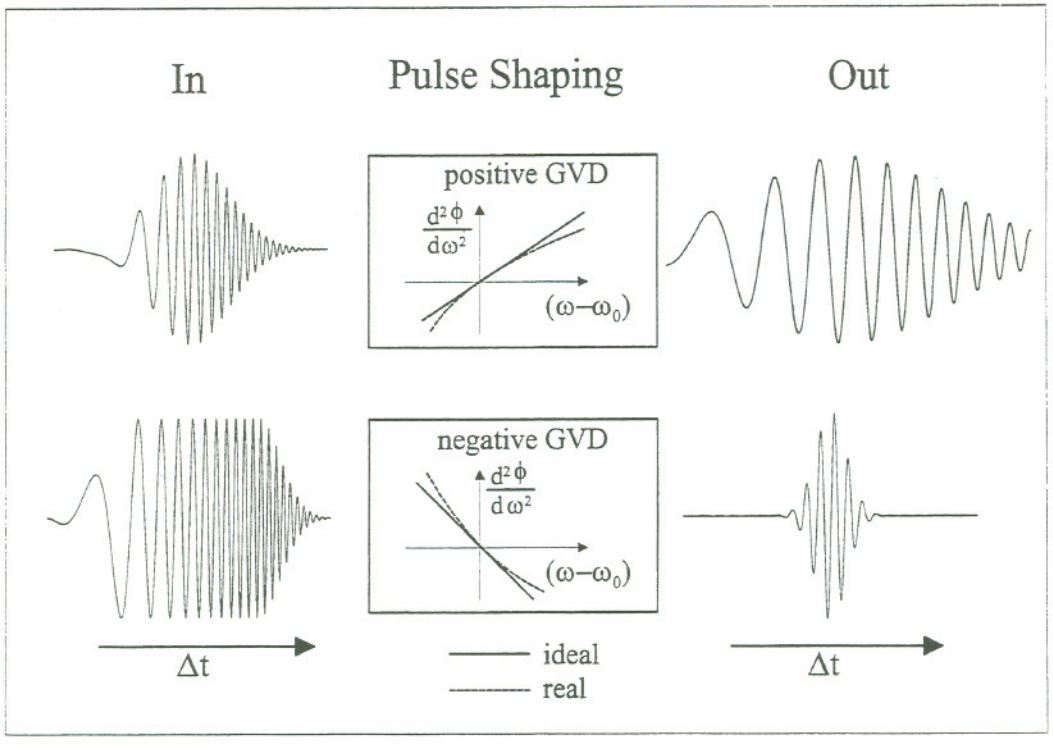

Figure IV.4: Different steps of pulse shaping. **Top:** A chirped pulses experiences GVD and broadens in time. **Bottom:** A chirped, broad pulse can be compressed to a short pulse by negative GVD (all frequency components "catch up" with each other).

IV.3 Experimental Part

Setup

We used gold-coated, holographic gratings with 1200 grooves/mm and 35% modulation depth for both stretcher and compressor. The angle of incidence was chosen 45° for the stretcher. This angle is easy to identify, and the diffraction efficiency is close to its maximum [60]. Under these conditions, we found the total efficiency for s-polarization at 820nm (including mirror losses) of the stretcher and compressor to be 40% and 55%, respectively. The telescope of the stretcher was set up with a gold-coated, parabolic mirror (f=44.45cm), and a flat mirror in the symmetry plane for compactness. An effective grating separation of 110mm stretches the output of the master oscillator to about 70ps. This is sufficient to avoid optical damage in the components of the amplifier.

Theoretical Simulation

We simulated the pulse propagation through the stretcher, amplifier gain medium, two SiO_2 AOMs and the compressor with a computer[3]. The results are diplayed in Fig IV.5. The straight lines in (a) reflect the ideal properties of the stretcher, which causes only second order dispersion (=linear group delay). To obtain the results in (b), 60 round trips of the seed pulse inside the amplifier were assumed. In this case, a total path length of 1920mm sapphire and 960mm SiO_2 had to be taken into account. The dispersion relations for sapphire and SiO_2 were taken from [51]. In an ideal system with only second order dispersion, the curve in (b) would be zero for all wavelengths. The remaining group delay is caused by third- and higher order dispersion, which can only to some extend be corrected in the compressor. From the simulations, we expected optimum performance with the compressor gratings 1.176× further apart than in the stretcher. This compensates for the second order dispersion in the amplifier cavity. Higher order effects can partially be compensated by varying the angle of incidence. The minimum pulse distortion occurs for γ=56.8°. Up to about 40nm bandwidth, higher order effects are small. For broader spectra, the pulse becomes more and more distorted. The same is true if the number of round trips in the amplifier cavity increases

[3]The original program was provided by B. Schoenlein. We then it modified for our application.

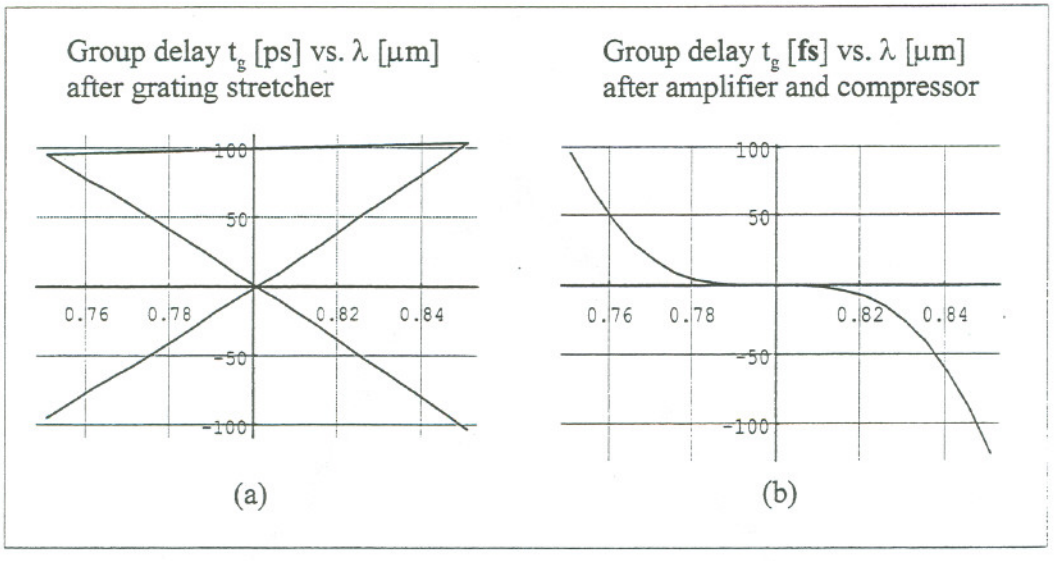

Figure IV.5: Theoretical simulation of the GVD in the stretcher, amplifier and compressor. (a) plots the relative group delay t_g over λ after the stretcher. (b) includes the dispersion of stretcher, 60 round trips in the amplifier and compressor.

significantly. Whereas the GVD can always be compensated, γ has obviously an upper limit. This restricts the amount up to which third-order dispersion can be accounted for.

Experimental Results

Experimental results are presented in Fig IV.6. The pulses from the master oscillator were stretched to about 70ps (a). This agrees well with the theoretical simulation for a 35nm wide pulse (see Fig IV.5 (a)). In a preliminary experiment, we bypassed the amplifier to test the performance of the compressor. The 68fs (FWHM) width of the autocorrelation corresponds to an intensity envelope of 56fs. Small deviations from the ideal Gaussian shape indicate residual uncompensated dispersion. This is confirmed by a time-bandwidth-product of

$$\Delta f_p \times \tau_p = 0.7$$

Owing the fact that no additional measures were taken to compensate for non-ideal behaviour of the compressor (finite spot size, higher-order dispersion) this result is adequate.

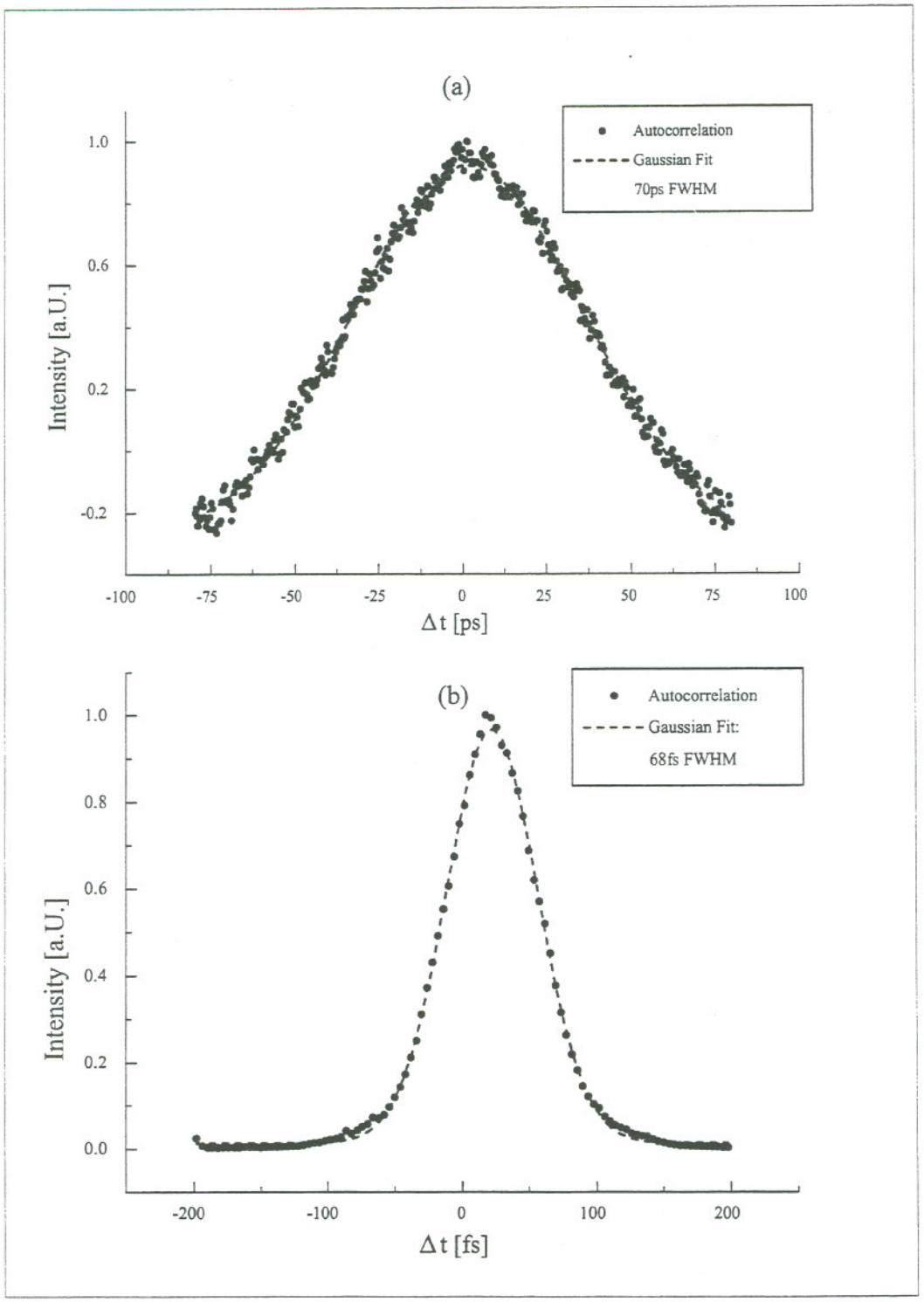

Figure IV.6: Experimental pulse stretching and compression. The autocorrelation of the pulse after passing the stretcher is shown in (a). To test the compressor, the amplifier was first bypassed and the pulse immediately recompressed (b).

Fig. IV.7 shows an autocorrelation of the final, amplified and recompressed pulse. The measurement yields a width of 96fs FWHM, assuming a Gaussian envelope function. The result was obtained with an angle of incidence of 59° for the compressor and ≈24cm grating separation. Both numbers are slighty larger than the theoretical predictions, which can be explained by additional dispersive elements (polarizing beamsplitter cube, Faraday rotator, telescope). It should be noted that successful recompression relies strongly on a fixed number of cavity round trips.

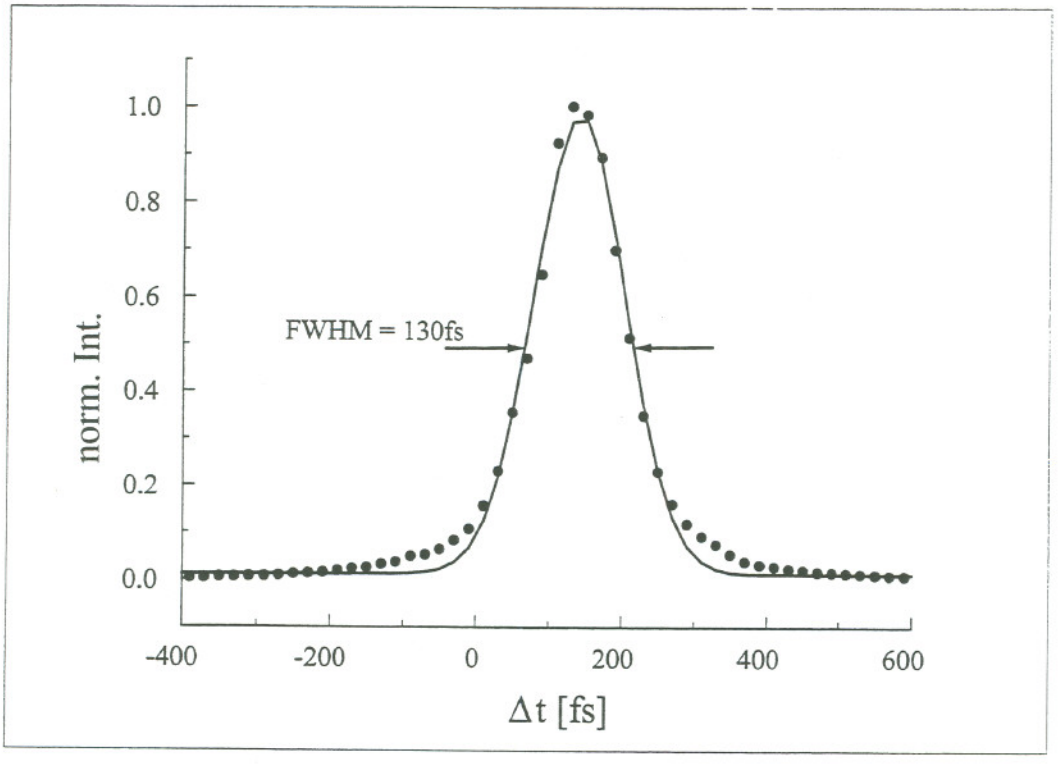

Figure IV.7: Autocorrelation of the amplified and recompressed pulse after 60 cavity round trips. Assuming a Gaussian shape, the pulse width is 96fs FWHM

The final angle of incidence of almost 60° caused a significant drop in the first order diffraction efficiency of the gratings. This resulted in a total compressor throughput of only about 10%. The low efficiency is in agreement with theoretical predictions and could only be avoided by already decreasing the angle of incidence into the stretcher or by using gratings with a higher groove density [49].

Chapter V

Regenerative Amplifier

After introducing the individual components of the amplifier in the previous chapters, we now describe their integration into a system.

The main link between seed laser and amplifier is the pulse switching mechanism. We use one acousto-optic device for both injection and cavity dumping. Because of its importance for the system, acousto-optic pulse manipulation is described in an own section. This includes both a theoretical treatment and a part which deals with design and configuration problems.

The overall amplifier system is introduced in the second part. A timing diagram explains the course of events (Q-switching, pulse injection, cavity dumping). The electrical setup and the optical layout are illustrated.

Experimental results about cavity dumping, pulse injection and amplifier operation are given in the last section.

V.1 Acousto-Optic Pulse Manipulation

In an acousto-optic (*ao*) device, light interacts with a traveling acoustic wave. Due to that process, the light can be deflected, diffracted or modulated. Acousto-optic interactions are divided into two classes: While the *anisotropic* effect alters the polarization of the light, the *isotropic* effect preserves it. Depending on the number of diffracted orders in the latter case, the deflection is either called *Bragg* (one diffracted order) or *Raman-Nath* (multiple diffraction orders).

For applications inside a laser cavity and at high repetition rates, acousto-optic modulators provide several advantages over electro-optic (*eo*) devices. In fact, thermally induced birefringence effects and acoustic ringing have limited electro-optically dumped regenerative amplifiers to repetition rates up to 10kHz [85]. Owing their lower insertion losses and the convenience of low-voltage operation, acousto-optical modulators are therefore the better choice at high repetition rates.

This section deals with both the theoretical and practical aspects of acousto-optic cavity dumping. The first part gives a theoretical background, whereas the second part concentrates on applied design considerations for effective cavity dumping.

V.1.1 Theory of Acousto-Optic Interaction

Acousto-optic devices are based on the photoelastic effect. An acoustic signal propagates through a crystal and produces regions of compression and expansion. The strain alters the optical properties of the material. As a consequence, a light beam passing through the crystal can be modulated or deflected. The general expression which relates the change in the index of refraction to the strain is:

$$\Delta\left(\frac{1}{n^2}\right)_{ij} = p_{ijkl}S_{kl}, \qquad i,j,k,l = 1,2,3. \tag{V.1}$$

Here, $\Delta(1/n^2)_{ij}$ is the change in the $(1/n^2)_{ij}$ component of the optical index ellipsoid, p_{ijkl} is the forth-rank photoelastic tensor, and S_{kl} are the strain components. Crystal symmetry determines which components of p_{ijkl} are non-zero and how components are related to each other.

If the acoustic wave has a periodical spatial profile, the repeated changes in the index of refraction create a phase grating for the light. Classical

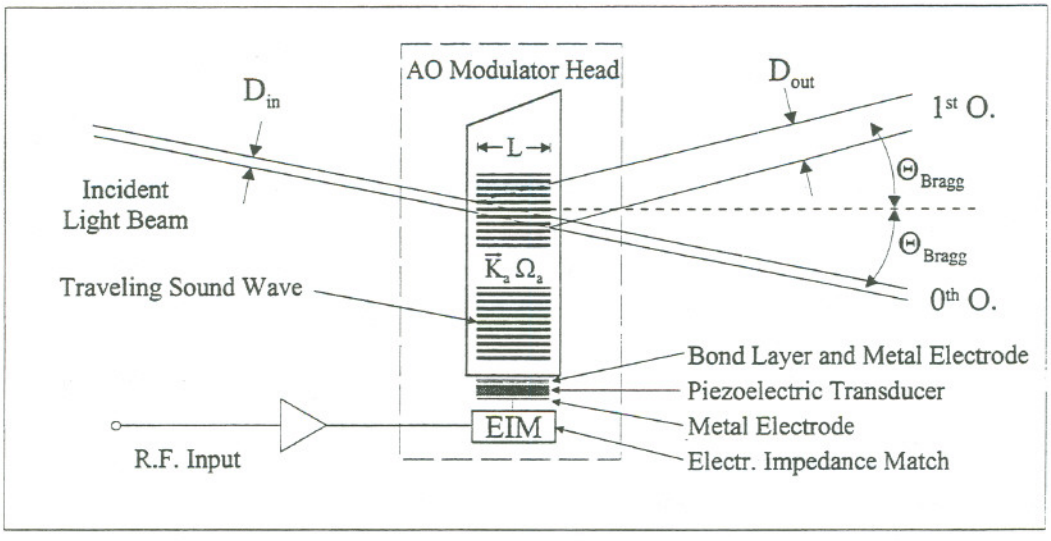

Figure V.1: Diagram of an acousto-optics modulator head

optics can describe the deflection process. The difference in this case is that the grating is not stationary; it travels with the speed of sound in the *ao* crystal. As one consequence, the deflected light is Doppler-shifted. To treat the problem mathematically, the wave equation has to be solved with a periodical change of the index of refraction. For an isotropic crystal, with the acoustic wave propagating along the x axis, and a monochromatic plane wave traveling in the xz plane at an angle Θ_0 (inside the medium) from the z axis, the wave equation can be written as:

$$\nabla^2 \mathbf{E} = \left[\frac{n(x,t)}{c}\right]^2 \frac{\partial^2 \mathbf{E}}{\partial t^2} \quad . \tag{V.2}$$

The planar, sinusoidal acoustic wave causes a change in the index of refraction according to

$$n(x,t) = n + \Delta n \sin\left(\Omega_a t - K_a x\right). \tag{V.3}$$

n is the average index of refraction, Δn is the amplitude of the strain-induced variation. Ω_a and K_a are the frequency and the wave number of the acoustic wave, respectively. Raman solved the problem in 1936 by expanding the electrical field in a Fourier series. He obtained:

$$\frac{dE_m}{dz} + \frac{u_1}{2L}\left(E_{m+1} - E_{m-1}\right) = i\left[\frac{m^2 Q}{2L} - mK_a \tan\Theta_0\right] E_m, \tag{V.4}$$

with the parameters defined as following: E_m is the amplitude in the m-th diffracted order, k_0 is the free-space and k_i the wave vector in the crystal. $u_1 = (-k_0 \Delta n L)/(\cos\Theta_0)$ is a coupling constant between adjacent orders, with L being the interaction length between optical and acoustical field. Q equals $(K_a^2 L)/k_i \cos\Theta_0)$ [42].

Only if the right-hand side of (V.4) is small for $m = \pm 1$, an appreciable amount of energy can be transferred from the zeroth into the $\pm$1st order. This is the case if either Q and $\tan\Theta_0$ are small, or if they are large but equal. The two cases correspond to the two diffraction regimes:

The interaction is of the Raman-Nath type if $Q \leq 0.3$ [23]. This condition requires a small value of L. Physically, the process corresponds to a diffraction of an optical beam at a thin, traveling grating. Therefore, multiple diffraction orders appear.

For $Q \geq 7$, the grating can no longer be regarded as thin. The diffraction is now in the Bragg regime. From the equality of the two expressions on the right-hand side of (V.4), we obtain for m=1 the Bragg condition:

$$\sin\Theta_0 = \sin\Theta_{Bragg} = \frac{K_a}{2k_i} = \frac{\lambda_0}{2n\Lambda}. \tag{V.5}$$

(Λ is the wavelength of the acoustic wave). The incoming beam is deflected at twice the Bragg angle (see Fig. V.1). In the Bragg regime, diffracted light predominantly appears in a single diffraction order. If we consider the interaction as a collision between a photon and a phonon, we see that momentum conservation requires the frequency of the diffracted light to be Dopppler-shifted. The relative direction between optical and acoustical beam determines the sign of the shift. The connection between the expression for the stress-induced index change (V.1) and the Raman solution (V.4) is in the Bragg regime given by the proportionality [76]

$$u_1 \propto (S_{kl} S_{kl}^*)^{1/2} \tag{V.6}$$

V.1.2 Design Considerations for AO Cavity Dumping

To find the most suitable *ao* device for a specific application, a number of parameters need to be considered. We list the ones which are most important

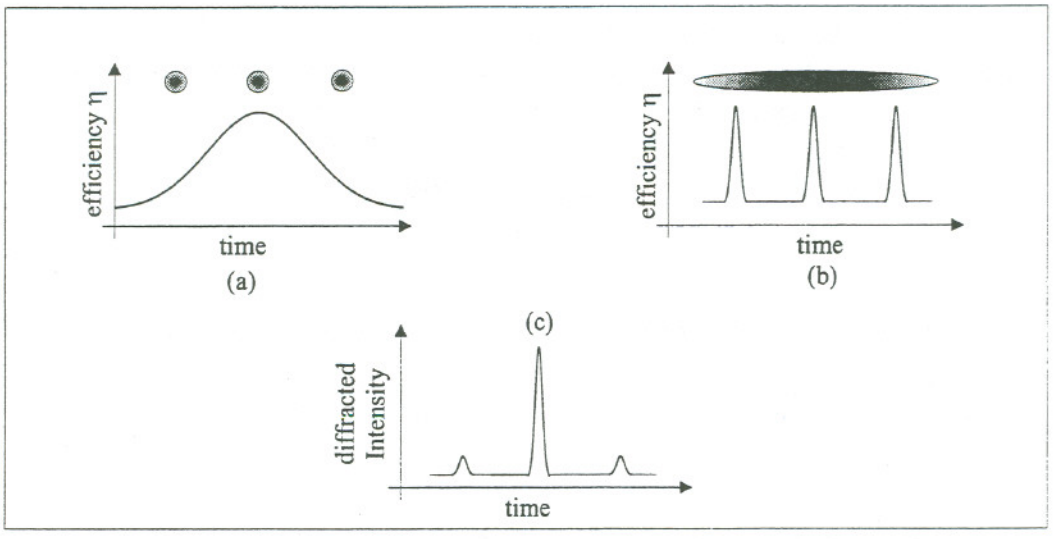

Figure V.2: Cavity dumping and limitation of the contrast ratio in repetitive cavity dumping. (a) shows a tightly focused optical spot, but the slow response of the cavity dumper (solid line) cause partial dumping of trailing and proceeding pulses. In (b), the spot size limits the contrast ratio even if the *ao* device is fast enough. Both (a) and (b) result in identical intensity vs. time diagrams (c).

for fast pulse switching in a regenerative amplifier:

Modulator Risetime and MTF: Pulses from the master oscillator arrive at the *ao* modulator at a 100MHz rate. Only a single one of them should be switched into the amplifier cavity. The acoustic field in the crystal can therefore be present only for a short time. Due to the limited speed of sound, this also corresponds to a small spatial extension of the sound field. On the other hand, to interact with the entire optical pulse, the spatial extension of the acoustic wave cannot be smaller than the optical spot size. It also takes a finite time for the leading edge of the sound field to pass an optical spot of given diameter. This time is a function of the spot size and the speed of sound in the material. For a Gaussian spot and very fast build-up time of the acoustic field, the modulated light profile has an analytical expression in form of an error function. The time interval it takes for the error function to rise from 10% to 90% is called the modulator rise time *for a given spot size.*

In reality, the response of the modulator to an applied RF pulse is not instantaneous. It is rather a convolution between the instrument response and the input signal. The modulation transfer function (MTF) allows to calculate the modulated light profile P as a function of the RF input signal V. In the frequency domain, it can be written:

$$P(f) = MTF(f) \times V(f) \tag{V.7}$$

Fig. V.2 illustrates how both a long risetime of the acoustic field and a large optical spot size can cause switching of more than one pulse into the cavity.

As a conclusion, fast response and efficient dumping ask for a modulator with a high speed of sound and/or tighter focusing of the laser beam.

Modulated light beam distortion: Fig. V.1 shows how due to a finite interaction length L the deflected beam has a larger cross section than the incident beam. The effect becomes increasingly stronger with smaller spot sizes and can result in a severely distorted beam profile [35].

Damage Threshold: For applications inside a laser cavity, the damage threshold of the material must have a high value—especially if effective dumping asks for a small optical spot size.

As it can be seen, the optical spot size and the material parameters of the *ao*-crystal need to be carefully balanced. The following table summarizes the properties of two widely used crystals, Tellurium Dioxide (TeO_2) and Fused Silica (SiO_2). Both allow a single-pass diffraction efficiency of $\approx 70\%$. Apart from the high necessary drive power, an SiO_2 cavity dumper performs better in all parameters.

Parameter	SiO_2	TeO_2
Damage Threshold	>1GW/cm^2	100MW/cm^2
Speed of sound ($\times 10^5$cm/sec)	6	4.2
Risetime (60μm spot)	6.4ns	9.1ns
Index of Refr. (at 630nm)	1.5	2.25
Typ. Peak Drive Power (W)	15	3

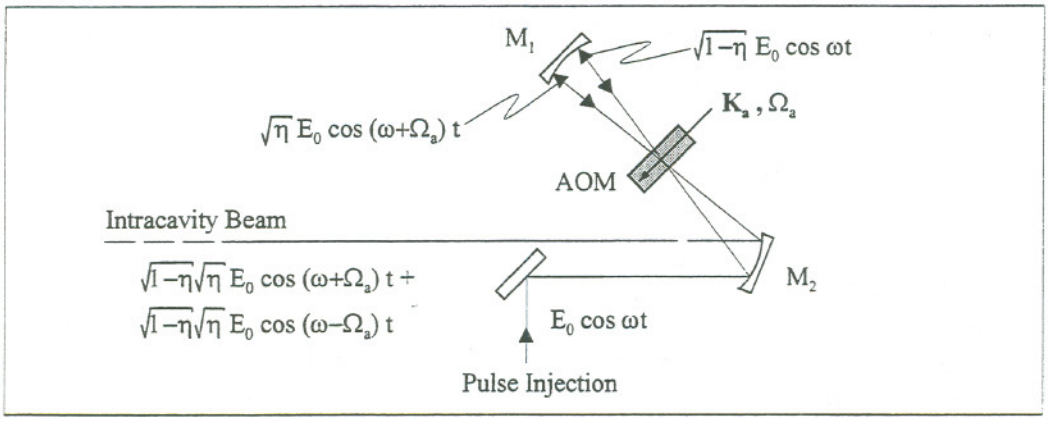

Figure V.3: Pulse injection using a double pass configuration and interferometric superimposition. For dumping out of the cavity, the two frequency components of the intracavity beam have to be considered.

V.1.3 Interferometric Cavity Dumping

As pointed out, the optical spot size is a critical parameter for efficient cavity dumping. The optimum spot size is a compromise between maximum allowable energy density in the cell, efficiency, rise time for the acoustic field and cavity design considerations.

A double pass optical geometry as shown in Fig. V.3 uses interferometrical combination of two beams to relax the spot size constraint. As detailed in the following, appropriate timing furthermore allows to suppress trailing and preceding pulses [34, 41] out of a train. The incident pulse can be described as $E_0(s,t)\cos\omega t$, where the pulse shape is described by $E_0(s,t)$ and varies slowly compared to the optical frequency. After a first interaction with the acoustic wave (frequency Ω_a), the diffracted light is Doppler-shifted and can be expressed as

$$\sqrt{\eta}E_0(s,t)\cos(\omega+\Omega_a)t. \tag{V.8}$$

η is the single-pass diffraction efficiency (i.e., $\eta = I_{diffracted}/I_{incident}$). The part of the pulse which passes through the AOM undeflected is reflected back by M_1 and can again interact with the acoustic wave on its way back. This contribution to the injected beam equals $\sqrt{\eta}\sqrt{1-\eta}\cos(\omega-\Omega_a)t$. The two parts add up to:

$$E(s,t) = \sqrt{\eta}\sqrt{1-\eta}\,E_0(s,t)\times[\cos(\omega+\Omega_a)t+\cos(\omega-\Omega_a)t] \tag{V.9}$$

Averaging over many optical cycles results in an intensity which is modulated at twice the acoustic frequency:

$$\boxed{I_{inject}(s,t) = 2\eta(1-\eta)\frac{E_0^2(s,t)}{2}(1+\cos 2\,\Omega_a t)} \qquad \text{(V.10)}$$

It can be seen from (V.10) that the injected intensity is maximized for η=0.5. Even more important is the $\cos 2\,\Omega_a t$ modulation term: If the acoustic frequency is chosen with an appropriate ratio to the pulse repetition rate, the modulation term equals zero when preceding and trailing pulses arrive.

The situation for dumping the pulse out of the cavity is slightly different, since the derivation starts from the intracavity pulse. Starting with (V.9) instead of $E_0 \cos \omega t$, we showed that the dumped intensity follows the same modulation pattern as (V.10):

$$\boxed{I_{dump}(s,t) = 4\eta^2(1-\eta)^2\frac{E_0^2(s,t)}{2}\left[(1+\cos 2\,\Omega_a t)\right]^2 .} \qquad \text{(V.11)}$$

V.2 Setup and Control

Having discussed all the individual components of the amplifier, we can now focus on the system as a whole. The timing scheme of the amplifier is outlined first. The second part describes the electronic control system for the amplifier. Finally, an optical setup plan gives an overview of the complete setup.

Timing Scheme

The timing scheme for the control of the regenerative amplifier is shown in Fig. V.4. Here, we want to illustrate only the course of events within one clock cycle. The technical realization is described after that.

Line(a): The master oscillator has a repetition rate of 103MHz. Its output is monitored by a fast photodiode.

Line(b): The repetition frequency of the seed laser is too high for the electronics. We use a discriminator to divide the signal down to 34MHz. This signal provides the "clock-input" for the timing electronics.

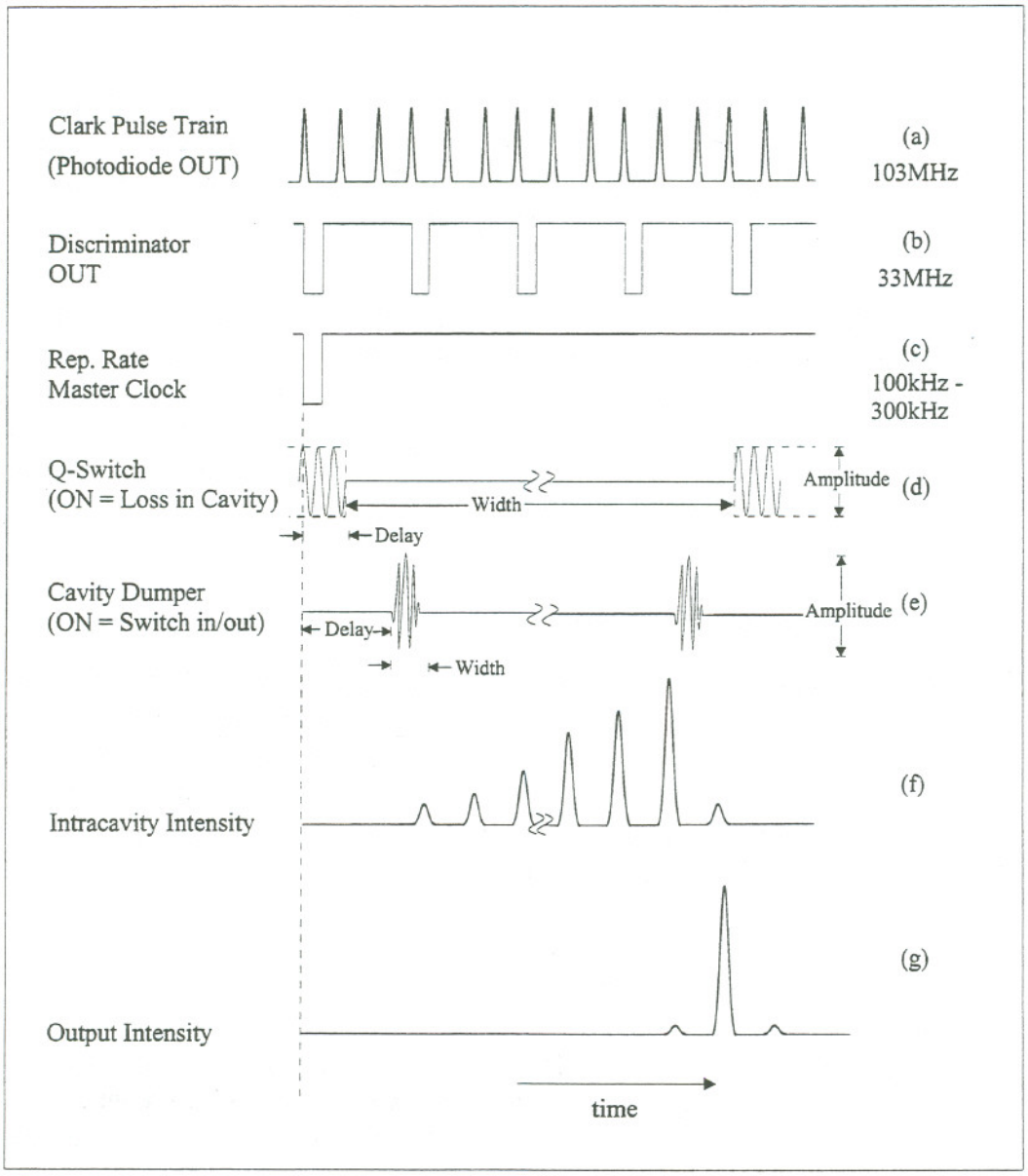

Figure V.4: Timing Scheme for the Amplifier System.

Line(c): With the clock signal as an input, the main component of the timing system sets a divider for the signal from the discriminator. This allows to adjust the repetition rate of the regenerative amplifier over a wide range.

Line(d): As long as the Q-switch driver provides a 80MHz RF signal, the cavity losses are high. This prevents the amplifier from lasing. To account for the finite opening time of the Q-switch, the RF signal is turned off shortly before an optical pulse is injected into the cavity.

Line(e-g): With a short (<9ns) burst of RF power applied to the cavity dumper, an optical pulse from the master oscillator is switched into the amplifier cavity. The pulse build-up is monitored with a photodiode. When the energy of the circulating pulse reaches its maximum, another RF signal dumps the amplified pulse. A fraction of it remains circulating in the cavity until the Q-switch suppresses lasing again.

V.2.1 Electronic Setup

The 103MHz pulse train from the master oscillator beats the time for the entire system. Since the actual timing system supports only inputs up to 50MHz, we use a discriminator to supresses two out of three pulses from the 103MHz signal. As an additional benefit, the discriminator delivers a standard output (NIM fast negative), which allows precise triggering. The 33MHz input into the timing system can be digitally divided down to any desired pulse repetition rate. Four output channels are available to drive external components. Two of them provide a gate signal for the Q-switch, the other two time injection and ejection of optical pulses. All outputs have a coarse (Δt=30.3ns) and fine (δt=0.12ns) time adjustment.

The Q-switch driver is controlled by the gate pulse from the timing system. Start, end and delay of the gate signal can be adjusted independently. While the gate signal is "on", a 80MHz, 4W RF signal is applied to the Q-switch, thus suppressing lasing of the amplifier.

The driver for the acousto-optic cavity dumper consists of two parts: The first stage delivers a 380MHz signal of variable duration, phase and power. The latter is limited up to 5.5W. The duration of the signal is adjusted to allow for efficient dumping, yet avoid switching of more than one optical

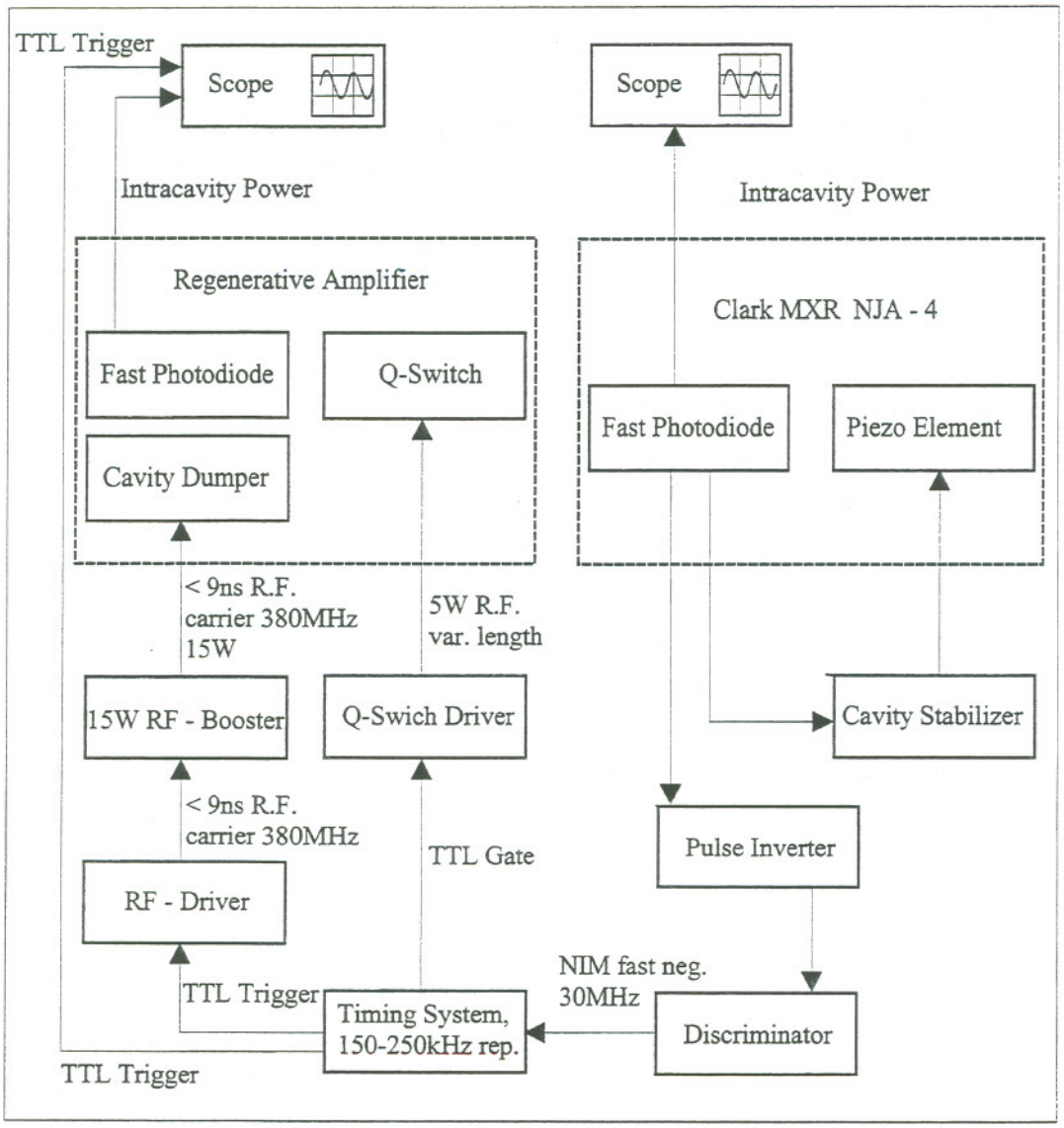

Figure V.5: Block diagram of the electronic driving system for the regenerative amplifier

pulse. The second stage is a broadband power amplifier which boosts the signal from the driver to max. 18W p-p.

The correct timing of all the signals as well as the pulse train inside the amplifier are controlled with an oscilloscope.

The Clark-MXR master oscillator uses a simple feedback loop to stabilize the mode-locking: One cavity end mirror is mounted on a piezo crystal. If the signal amplitude from the monitoring photodiode falls below an (adjustable) threshold, vibrations of the back mirror provide a small perturbation to the cavity. This is supposed to re-establish modelocking. In most cases however, we found the perturbation by the piezo mounted mirror insufficient. In addition, the laser cavity frequently required major re-alignment to start modelocking.

V.2.2 Optical Design

An overview over the complete optical setup is given in Fig. V.6. The pulses from the master oscillator enter the stretcher from the top of the drawing. Mirror S1 is cleared vertically by the incoming beam. After passing the stretcher (described in detail in the previous chapter) with a small vertical offset, the pulses are deflected by S1. In order to obtain a small spot size inside the cavity dumper and good mode-matching of the injected beam, we use a telescope (TEL1). The three following optical components are a polarizing beamsplitter cube (PBSC), a Faraday rotator (FR) and $\lambda/2$ waveplate. Together, they form an optical isolator: The injected beam passes without an alteration of the polarization. This is not true for the pulses ejected from the amplifier—the waveplate and the Farady rotator change the polarization 90° with respect to its original, horizontal orientation. Now being vertically polarized, the beam is deflected to the left by the beamsplitter cube.

In the amplifier, incoming pulses are deflected towards the cavity dumper (CD) by M6. A slight angular deflection in the AOM (twice the Bragg-angle) injects the pulses into the cavity. The latter is formed by the mirrors M1-M5, the SiO_2 Q-switch (QS) and the cavity dumper (CD). A photodiode (PD1) monitors the intracavity power through a small leakage of M1. Master Oscillator (not shown) and amplifier are pumped by the shared output of a large-frame argon ion laser. The typical 16W output is split in a 3:1 ratio. 4W pump the seed laser, 12W are directed into the amplifier through the Lens L1 (f=132mm). After switching the pulses out of the amplifier, they are deflected by PBSC and enter the compressor. A second telescope (TEL2)

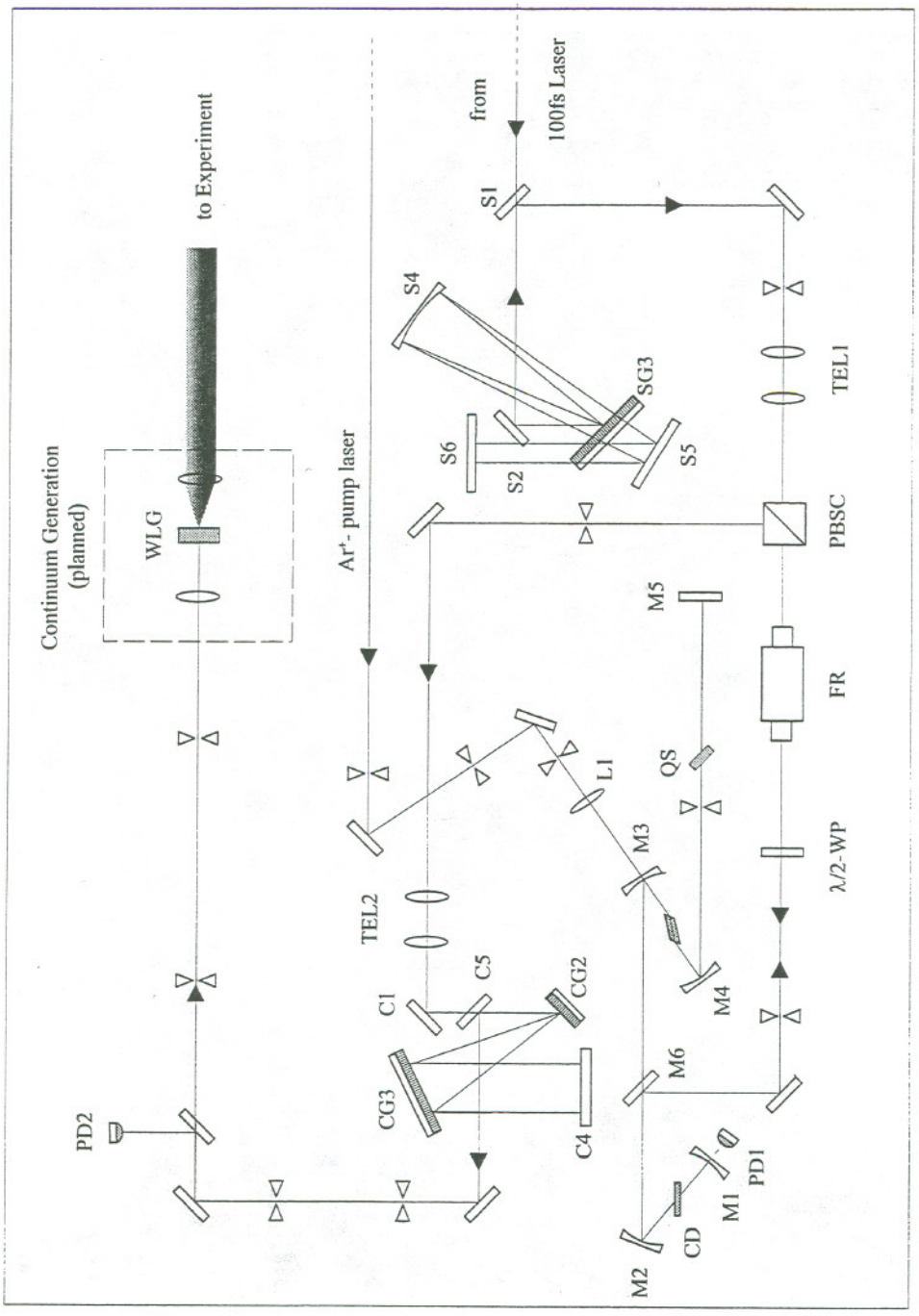

Figure V.6: Optical setup of the regenerative amplifier system. The actual amplifier cavity (M1-M5) is located in the lower right corner. S1-S6 form the stretcher, with SG3 being the grating and S4 the parabolic mirror. The compressor is formed by C1-C5. CG2 and CG3 are gratings.

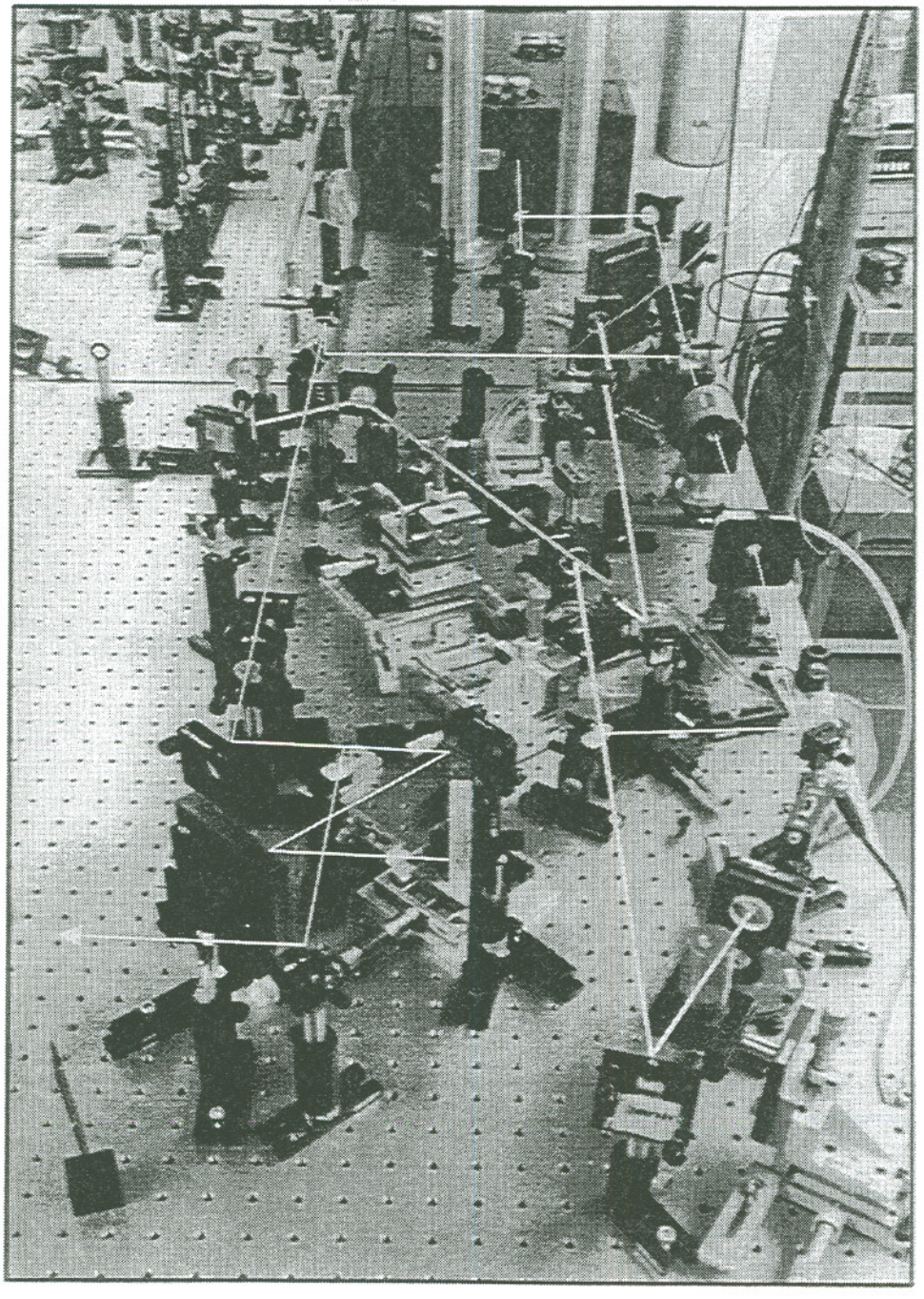

Figure V.7: Photograph of the optical setup. A description is given in the text.

collimates the beam. Again, a small vertical offset allows to use a pick-off mirror C5 (The operating principle of the compressor is described in the previous chapter).

Fig V.7 is photograph of the complete system. The master oscillator laser (back) is enclosed. The pump source is mounted on top of the system; only two posts are visible. Narrow white lines highlight the beampaths to and from the amplifier; a bold white line the intracavity path. For simplicity, we did not draw the beamline through the stretcher. The pump heam is highlighted by a grey line.

V.3 Experimental Setup and Results

All the experiments described below were carried out using the final setup of the amplifier system.

V.3.1 Cavity Dumping

We first used a TeO_2 AOM for cavity dumping. Data from testing the device in the final setup (Fig. V.6) are displayed in Fig. V.8. The cavity was operated Q-switched, with the intracavity power being monitored with PD2 (fast Si-detector) The cavity dumped pulse was picked of by M6 and directed into a second photodiode. The profile of a cavity dumped pulse together with the intracavity power are shown.

At the peak of the Q-switched pulse, a burst of RF power (FWHM=15ns, 5W peak) is supplied to a TeO_2 AOM. Immediately, the intracavity power drops sharply. The step corresponds to a diffraction efficiency of about 50%. As shown in (V.10), this value constitutes the optimum for interferometric cavity dumping The dumped pulse (dashed line) has a duration (FWHM) of 20ns; 30% longer than the RF excitation. Together with the low efficiency, this leads to the conclusion that the TeO_2 dumper did not respond fast enough to the RF signal. Indeed, for inputs between 6ns and 20ns, the length of the dumped pulse did not change significantly. The slow response of the TeO_2 cell is in general attributed to a bad impedance match between the $LiNbO_3$ transducer and TeO_2. It results in a restricted bandwidth and therefore a slower response.

For that reason, the TeO_2 AOM was later replaced by a SiO_2 device.

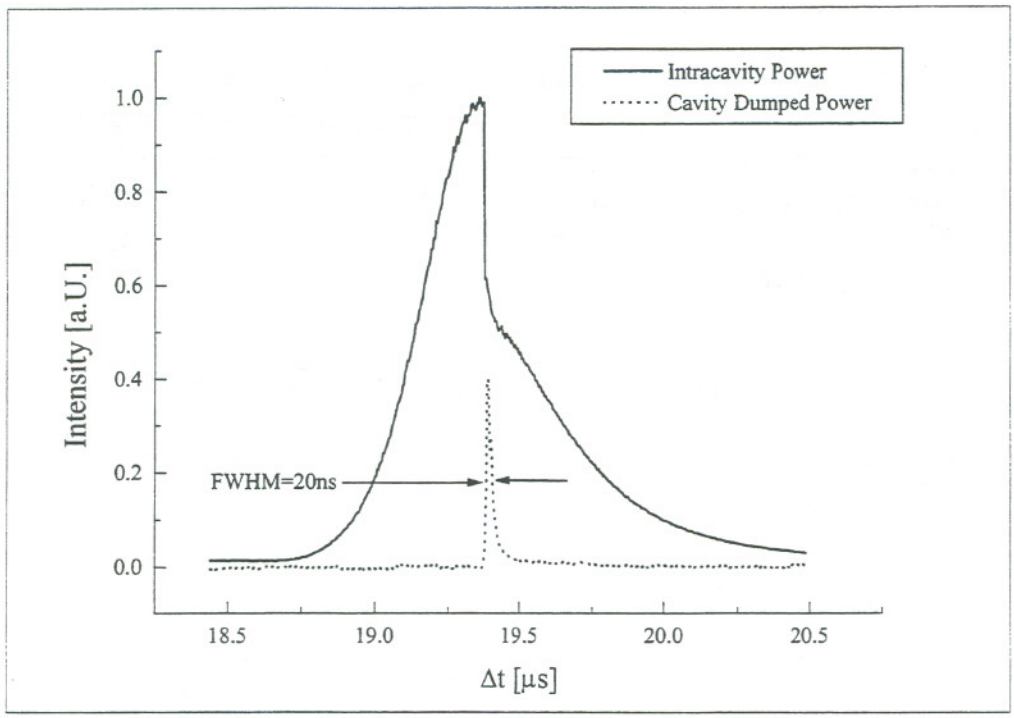

Figure V.8: Cavity dumping of a Q-switched laser pulse. Since two different diodes were used to monitor intracavity and dumped intensity, the measured intensities are not directly comparable. The pulse trains were recorded with a digital sampling scope and read out data over the IEEE 488 port.

Pulse Injection: Results obtained with the SiO_2 cavity dumper are shown in Fig V.9. Here, we measured the injection of pulses from the master oscillator into the amplifier cavity. To obtain the data, a fast photodetector was placed inside the amplifier cavity: We verified a sufficiently small optical spot size with both theoretical calculations and through a "knife-edge" measurement. The limitation imposed by the response of the *ao* device can be observed. Not only the main pulse, but also leading and trailing pulses are at least partially switched into the cavity. Knowing their ratio of 11.5:1 and the time between the pulses ($\Delta t = 1/f_{rep} = 8.83$ns), the response of the AOM can be determined. If a Gaussian shape is assumed, the FWHM of the acoustic

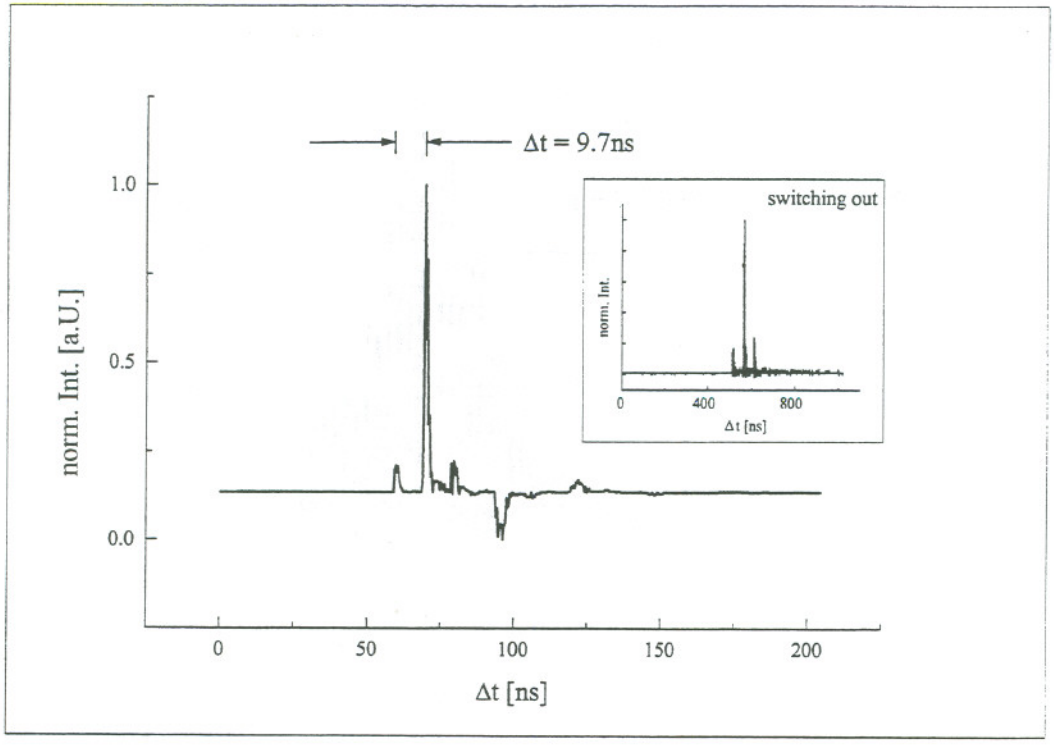

Figure V.9: Pulse injection into the amplifier cavity. Leading and trailing pulses are due to the residual acoustic wave. The exciting RF pulse had a length of ≈4.5ns FWHM. The temporal resolution is limited by the risetime of the detector (≈1ns).

wave calculates to

$$\tau_{AOM}^{min} = 9.41ns \quad \text{(FWHM)} \tag{V.12}$$

This value agrees with the specifications of the manufacturer. The better suppression ration of existing systems (>100:1 using the same cavity dumper) [37,50,59] can be explained by lower repetition rates of their seed lasers. With f_{rep}=76MHz and the value from (V.12), the amplitude of the acoustic wave drops already to 1/225 of its maximum.

V.3.2 Amplifier Operation

A typical pulse train, as detected with a fast photodiode through M1, is shown in Fig V.10. About 1nJ of pulse energy are switched into the amplifier

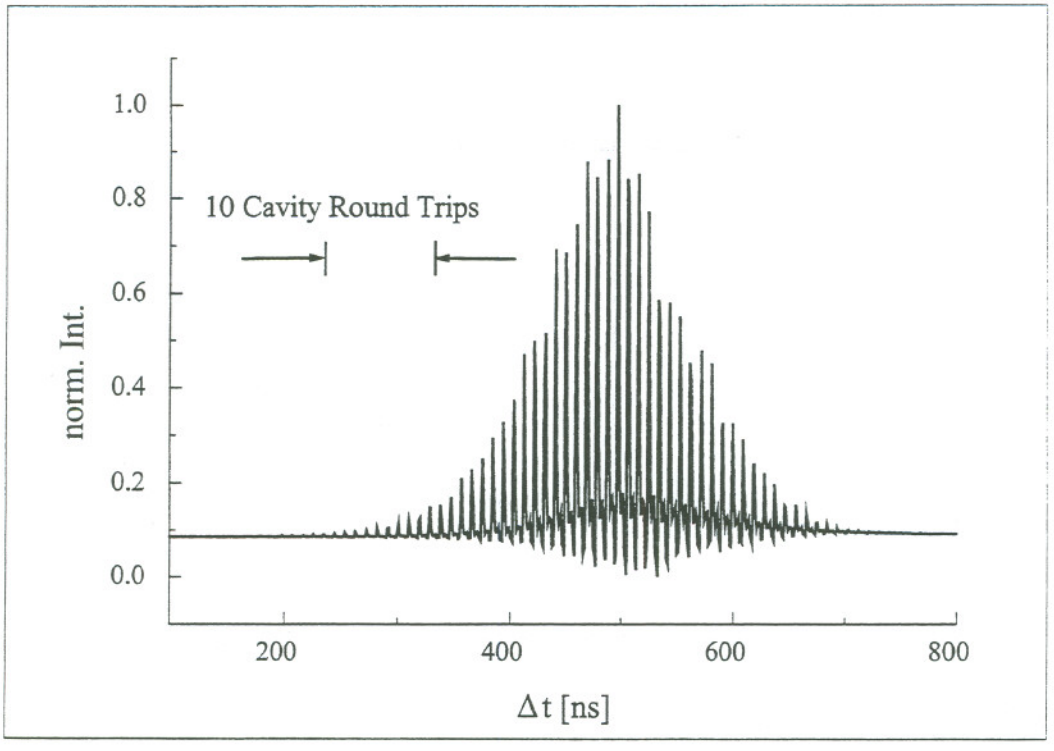

Figure V.10: Build-up of a pulse inside the amplifier resonator. The large peak-to-peak fluctuations are due to the finite sampling rate of the scope.

cavity. After 60 round trips, the gain in the crystal is depleted, and typically 1.5μJ are dumped out of the amplifier. This corresponds to an averaged single pass gain of 7.5%. Although the number is low compared to our single pass measurements, it agrees with previously published results [58]. Also, the results in Chapter 2 were achieved in the small-signal limit, which holds certainly no longer true in the case of the amplifier. Table ?? summarizes the final performance of the amplifier system. "Typical" values could be achieved with only minor alignment.

V.4 Discussion and Outlook

We have planed, designed and built a Ti:sapphire regenerative amplifier. The performance of the final system has been shown to be consistent with the calculations and preliminary experiments. It has been demonstrated that

Parameter	Optimum	Typical
Pulse duration (FWHM)	96fs	150fs
Pulse Engery	1.9μJ	1.5μJ
Average Power	280mW	230mW
Contrast Ratio	8:1	6:1

Table V.1: Amplifier performance with 13.5W pump power and 150kHz repetition rate, measured before recompression.

nJ pulses from the master oscillator can be amplified to the μJ level and recompressed to sub-100fs duration.

A comparison of our accomplishments with published results [58] and the only commercially available system (*Coherent RegA9000*) show that despite the already good performance, improvement is possible in two aspects.

First, the switching into and dumping out of the amplifier can be done with a better ratio between main and side pulses. The inferior switching contrast ratio of our system, however, is a direct consequence of the high repetition rate of the master oscillator and therefore inherent in the present setup. Extending the cavity length of both the master oscillator and the amplifier can solve the problem. Already an 0.5m longer laser cavity lowers the repetition rate by 1/3, which should yield a 20$\times$ better switching contrast.

Second, we pointed out in the previous chapter that the total efficiency of the compressor decreases sharply for higher angles of incidence. Since the final pulse energy is crucial for continuum generation, losses in the compressor should be minimized. This can be achieved by slightly changing the design of the stretcher/compressor combination: Chosing an angle of incidence closer to the Littrow angle will result in a higher grating reflectivity. An increase of the total efficiency by a factor of 5 seems possible.

As a conclusion, we suggest three changes of the current regenerative amplifier. The combination of them will help to further optimize the performance of the system.

- Reconstruction or replacement of the of the master oscillator to lower the repetition rate. This will improve the switching contrast ratio significantly.
- Realignment of stretcher and compressor for a smaller angle of incidence. It should be possible to increase the efficiency of the compressor by a factor of 5.
- Full enclosure of the amplifier cavity to eliminate the noise caused by air currents. Ultimately, the noise of the overall system should be limited by the noise of the pump laser.

Appendix A

A.1 Continuum Generation

Continuum generation is one of many fascinating nonlinear optical effects. The effect arises from the propagation of an intense ultrashort laser pulse through matter. A strong electrical field interacting with the material can change the index of refraction. This variation is caused by the nonlinear contribution n_2 to the total index of refraction n. The refractional change in turn modifies phase and amplitude of the propagating signal. This process feeds itself through nonlinear mixing and ultimately broadens the frequency spectrum of the output pulse considerably.

The first section focuses on the mechanisms which give rise to continuum generation in general. Since no comprehensive theoretical model is presently available, the discussion is limited to qualitative arguments. The most important contributor to the effect—Self Phase Modulation or SPM—is then studied in more detail. Again, we will restrict ourselfs mainly to a qualitative study. The derivation of a theoretical model for SPM [88] is given at the end. Even if the model is limited to a special case, it was shown to be in good agreement with earlier experimental results [21]. The difficulties entountered for obtaining a better model are also mentioned.

A.1.1 Mechanisms for Continuum Generation

Various effects are responsible for the wide spectral broadening of the pulse. Among the ones discovered so far are self-, induced- and cross-phase modulation as well as four-photon parametric generation.

- A phase change can cause a frequency sweep within the pulse envelope due to the nonlinear part of the index of refraction n_2. This effect is called self-phase-modulation (SPM) and was discovered already in the early days of nonlinear optics [7, 71, 79]. SPM is discussed in greater detail below.

- Photons at the laser frequency can create other photons at Stokes and anti-Stokes frequencies through parametric interaction. These photons are emitted in angular patterns determined by phase matching conditions.

- Interaction between light and phonons is another source for the generation of new frequency components: When a coherent vibrational mode is excited by the laser, stimulated Raman scattering can occur. The stimulated Raman scattering also couples with SPM. The different frequencies created by Raman scattering and SPM can interfere and change the emission pattern. This effect is called *stimulated Raman scattering cross-phase modulation* [22].

- In a medium with non-vanishing $\chi^{(2)}$ and a strong $\chi^{(3)}$, SHG and SPM can couple together. Here again, interference between the two effects changes the emission spectrum (*second harmonic generation cross-phase modulation)*

Self Phase Modulation

SPM is the initiator and major contributor to continuum generation. As mentioned already above, the physical origin of the effect lies in an intensity dependant change of the index of refraction. Feedback of the media on the beam causes a sweep in frequency.

In the following, we list some major effects which contribute to the change of the nonlinear index of refraction n_2:

Electronic Mechanisms An eletrical field mixes the electronic wavefunctions, shifts the energy levels and redistributes the population. All these effects can contribute to the induced change of the refractive index. Close to an optical absorbtion band, the effects can be resonantly enhaced. In a very strong field, saturation effects and multiphoton absorbtion become increasingly important. The response times are usually fast ($10^{-14} - 10^{-15}$s); only a population redistribution takes place on a longer timescale.

Vibrational Contribution The laser field can also mix the vibrational wave functions, shift the energies and redistribute the population of the phonons. These effects, however, are many (~ 5) orders of magnitude smaller than the electronic contributions. Consequently, this contibution is only significant for lasers in the IR, where vibrational resonances can be excited.

Rotation and Molecular Reorientation Especially in liquids, Raman excitation of molecular rotations can contribute to n_2. In the solid state, the rotation is strongly impeded by the next neighbours. Instead of rotating, molecules can now vibrate in their potential well which, too, can increase n_2.

Other Effects A number of other mechanisms can play a role in changing the nonlinear index of refraction. Among them are: Electrostriction, laser heating, photorefraction and molecular redistribution. Due to the slow response time of the processes, they can only contribute significantly for pulses longer than 100ns. The shorter the laser excitation is, the more dominant are electronic effects.

To conclude, it can be said that due to the extremely high electrical fields which are typically involved in continuum generation, a large number of nonlinear interactions can take place. These interactions often couple together—which creates even more of them.

Together with SPM *in time*, a closely related spatial effect usually occurs. Since the laser beam has a finite cross section—and therefore a transverse intensity profile—SPM has a transversal dependance as well. As a result of spatial profile of n, the beam is self-diffracting. Such a self-diffraction, resulting from SPM *in space*, is responsible for self-focusing and self-defocusing [52,69].

Temporal and spatial SPM are in general hard to separate, which makes the independant study of both cases difficult. The problem can be avoided

by coupling the laser pulse into a fiber [80]. Here, the wave is guided and the cross section of the beam remains constant. Self-focusing does not occur, thus allowing the study of "pure" temporal SPM.

On the other hand, self focusing can be quite desirable. In fact, it is true for most practical cases that self-focusing starts at lower intensities and before self-phase modulation becomes appreciable. [70]. Only then, the self induced convergence of the beam leads to a significant increase in the power density, which in turn induces a strong SPM in time.

A.1.2 Theory of SPM (Yang, 1984)

The propagation of a laser pulse in an isotropic medium with vanishing $\chi^{(2)}$ can be described by the wave equation:

$$\left(\frac{\partial^2}{\partial z^2} - \frac{n_0^2}{c^2}\frac{\partial^2}{\partial t^2}\right)\mathbf{E} = \frac{4\pi}{c^2}\frac{\partial^2}{\partial t^2}\mathbf{P}^{(3)} \tag{A.1}$$

For the laser pulse, the treatment is restricted to only one dimension. Also, the optical field is assumed to be far from resonance. Excitations are therefore all virtual and instantaneous in response. This allows to write:

$$\mathbf{E} = E \equiv \mathcal{E}(z,t)\exp\left(ik_0 z - iw_0 t\right) \tag{A.2}$$

$$P^{(3)} = \chi^{(3)}\left|E\right|^2 E. \tag{A.3}$$

Yang [88] showed that by defining the operators $\hat{\mathsf{D}}_{\pm} \equiv (\partial/\partial z) \pm (n_0 c)(\partial/\partial t)$ and $\Pi = -\frac{4\pi\omega_0^2}{c^2}\left[1 + \frac{2i}{\omega_0}\frac{\partial}{\partial t} - \frac{1}{\omega_0^2}\frac{\partial^2}{\partial t^2}\right]\chi^{(3)}\left|\mathcal{E}\right|^2\mathcal{E}$, the wave equation (A.1) can be written in a very compact way as a power series:

$$\begin{aligned} 2ik_0\hat{\mathsf{D}}_+\mathcal{E} &= -\hat{\mathsf{D}}_-\left(\hat{\mathsf{D}}_+\mathcal{E}\right) + \Pi \\ &= \sum_{m=0}^{\infty}\left[\left(-\frac{\hat{\mathsf{D}}_-}{2ik_0}\right)^m \Pi\right]. \end{aligned} \tag{A.4}$$

It should be noted that up to that point, no approximations were made. In particular, the derivation does not rely on the "slowly changing envelope" assumption [1]. Having the solution as a series, it is a only a question of how many terms are inlcuded to better describe SPM

[1] This often used simplification assumes a slowly varying envelope function in order to neglect higher derivatives of it. However, a theory of SPM should cover exactly the situation of short pulses

To obtain the zeroth order solution, all derivatives of $\chi^{(3)} |\mathcal{E}|^2 \mathcal{E}$ are neglected. The resulting first-order differential equation yields two important results:

$$\boxed{|\mathcal{E}| = |\mathcal{E}(t)| \quad (\text{and} \neq f(z)).} \tag{A.5}$$

This shows that the pulse propagates in the medium without any distortion of its shape. From the result of the spatial phase development, the spectral broadening is given by integrating over z and using $\Delta\omega(t) = -\partial\phi/\partial t$

$$\boxed{\Delta\omega(t) = -\frac{2\pi\omega_0^2}{c^2 k_0}\chi^{(3)}\frac{\partial |\mathcal{E}|^2}{\partial t}z.} \tag{A.6}$$

The main feature of the next higher order solution is that the solution for $\partial\mathcal{E}/\partial z$ is no longer zero. This causes a pulse shape deformation during pulse propagation. The phenomena is refered to as *pulse steepening.*

In fact, the first order solution decribes a strong *temporal* SPM fairly well [70]. Practically, this situation can only be achieved in fibers or in extremely thin samples, where *spatial* effects such as self-focusing can be neglected.

However, since in most cases self-focusing effects do come into play, a complete theory of SPM is very difficult. This is mainly due to the fact that a quantitative theory of self focusing is not yet availabale. A theoretical understanding of *continuum generation*, where SPM is only one contributor among many others, is consequently far from being developed.

Bibliography

[1] G. Albecht, J. Eggleston, and J. Ewing. Measurements of Ti:sapphire as a lasing material. *Opt. Comm.*, 52(6):401–404, January 1985.

[2] R. R. Alfano. *The Supercontinuum Laser Source.* Springer Verlag, New York, 1989.

[3] R. R. Alfano and S. L. Shapiro. Emission in the region 4000-7000Å by four-photon coupling in glass. *Phys. Rev. Lett.*, 24:584, 1970.

[4] M. T. Asaki, C. P. Huang, D. Garvey, J. Zhou, H. C. Kapteyn, and M. M. Murnane. Generation of 11fs pulses from a self mode locked Ti:sapphire laser. *Opt. Lett.*, 18(12):977–980, June 1993.

[5] S. Bar-Ad, P. Kner, M. V. Marquezini, and D. S. Chemla. Carrier dynamics in the quantum kinetics regime. *Phys. Rev. Lett.*, 77(15):3177–3180, October 1996.

[6] J.-Y. Bigot, M.-A. Mycek, S. Weiss, R. G. Ulbrich, and D. S. Chemla. Instantaneous frequency dynamics of coherent wave mixing in semiconductor quantum wells. *Phys. Rev. Lett.*, 70(21):3307–3310, May 1993.

[7] N. Bloembergen and P. Lallemand. Complex intensity-dependant index of refraction, frequency broadening of stimulated raman lines, and stimulated raleigh scattering. *Phys. Rev. Lett.*, 16:81, 1966.

[8] G. D. Boyd and H. Kogelnik. Generalized confocal resonator theory. *Bell Sys. Tech. J.*, 41:1347–1369, July 1962.

[9] R. E. Bridges, R. W. Boyd, and G. P. Agrawal. Multidimensional coupling owing to optical nonlinearities. *J. Opt. Soc. Am. B*, 13(3):560–569, March 1996.

[10] C. Byvik and A. Buoncristani. Analysis of vibronic transitions in titanium doped sapphire using the temperature of the fluorescence spectra. *IEEE J. Quantum Electron.*, QE-21(10):1619–1623, October 1985.

[11] I. P. Christov, H. C. Kapteyn, M. M. Murnane, C.-P. Huang, and J. Zhou. Space-time focusing of femtosecond pulses in a Ti:sapphire laser. *Opt. Lett.*, 20(3):309–311, February 1995.

[12] S. Cundiff, M. Koch, W. H. Knox, J. Shah, and W. Stolz. Coherent exciton-continuum coupling in semiconductors. In *QELS 1996 - Technical Digest*, pages 105–106, Washington, 1996. Optical Society of Amerika.

[13] S. T. Cundiff, W. H. Knox, E. P. Ippen, J. Khatri, and H. A. Haus. Frequency dependent mode size in Kerr-lens mode-locked lasers. In *CLEO '96, Technical Digest Series, Conference Edition*, volume 9, pages 25–26, Washington, June 1996. Optical Society of America.

[14] P. F. Curley, Ch. Spielmann, T. Brabec, F. Krausz, E. Winter, and A. J. Schmidt. Operation of a femtosecond Ti:sapphire solitary laser in the vicinity of zero group-delay dispersion. *Opt. Lett.*, 18(1):54–56, January 1993.

[15] L. Davis. Theory of electromagnetic beams. *Phys. Rev. A*, 19:1177–1179, March 1979.

[16] A. J. DeMaria, C. M. Ferrar, and G. E. Danielson. Mode locking of a Nd^{3+}-doped glass laser. *Appl. Phys. Lett.*, 8(1):22–26, January 1966.

[17] M. DiDomenico. Small signal analysis of internal (coupling type) modulation of lasers. *J. Appl. Phys.*, 35:2870–2876, October 1964.

[18] R. L. Fork, C. H. Brito Cruz, P. C. Becker, and C. V. Shank. Compression of optical pulses to six femtoseconds using qubic phase correction. *Opt. Lett.*, 12(7):483–485, July 1987.

[19] R. L. Fork, G. H. C. Greene, and C. V. Shank. Generation of optical pulses shorter than 0.1psec by colliding pulse mode locking. *Appl. Phys. Lett.*, 38(9):671, May 1981.

[20] R. L. Fork, O. E. Martinez, and J. P. Gordon. Negative dispersion using prisms. *Opt. Lett.*, 9(5):150–152, May 1984.

[21] R. L. Fork, C. V. Shank, C. Hirlimann, and R. Yen. Femtosecond white-light continuum pulses. *Opt. Lett.*, 8:1, 1983.

[22] J. Gersten, R. Alfano, and M. Belic. Combined stimulated raman scattering in fibers. *Phys. Rev. A*, 21:1222–1224, 1980.

[23] A. P. Goutzoulis and V. P. Kludzin. Principles of acousto-optics. In A. P. Goutzoulis and D. R. Pape, editors, *Design and Fabrication of Acousto-Optic Devices*, Optical Engineering, pages 1–68, New York, 1994. Marcel Dekker, Inc.

[24] D. Hanna. Astigmatic Gaussian beams produced by axially asymmetric laser cavities. *IEEE J. Quantum Electron.*, QE-5(10):483–488, October 1969.

[25] R. L. Hargrove, R. L. Fork, and M. A. Pollack. Locking of HeNe laser modes induced by synchronous intracavity modulation. *Appl. Phys. Lett.*, 5:4–5, July 1964.

[26] S. E. Harris and O. P. McDuff. Theory of FM laser oscillation. *IEEE J. Quantum Electron.*, QE-1:245–262, 1965.

[27] H. A. Haus. Theory of mode locking with a fast saturable absorber. *J. Appl. Phys.*, 46:3049–3068, July 1975.

[28] H. A. Haus. Parameter ranges for cw passive mode locking. *IEEE J. Quantum Electron.*, QE-12:169–176, March 1976.

[29] H. A. Haus, J. G. Fujimoto, and E. P. Ippen. Analytical theory of additional pulse and Kerr lens mode locking. *IEEE J. Quantum Electron.*, 28:2086, 1992.

[30] H. A. Haus, C. V. Shank, and E. P. Ippen. Shape of passively mode-locked laser pulses. *Opt. Commun.*, 15:29–31, September 1975.

[31] E. Hecht and A. Zajac. *Optics*. Addison-Wesley, Massachusetts, 4 edition, 1979.

[32] D. Huang, M. Ulman, L. H. Acioli, H. A. Haus, and J. G. Fujimoto. Self focusing induced saturable absorber loss for laser mode locking. *Opt. Lett.*, 17(7), April 1992.

[33] F. A. Jenkins and H. E. White. *Fundamentals of Optics.* McGraw-Hill, 1957.

[34] R. H. Johnson. Characteristics of cavity dumping in a mode locked laser. *IEEE J. Quantum Electron.*, QE-9:255–257, February 1973.

[35] R. V. Johnson. Design of acousto-optic devices. In A. K. Goutzoulis and D. P. Pape, editors, *Design and Fabrication of Acousto-Optic Devices*, pages 123–196, New York, 1994. Marcel Dekker, Inc.

[36] C. Jorgenson. Comparative ligand field studies IV. *Chem. Scand.*, 11:73–85, 1957.

[37] Rhee June-Koo, T. S. Sosnowski, T. B. Norris, J. A. Arns, and W. S. Colburn. Chirped-pulse amplification of 85fs pulses at 250kHz with third-order dispersion compensation by use of holographic transmission gratings. *Opt. Lett.*, 19(19):1550–2, 1994.

[38] J. D. Kafka and T. Baer. Multimode mode locking of solid state lasers. In *Conference on Lasers and Electrooptics (CLEO)*, Baltimore, MA, 1991. Optical Society of Amerika. Talk JMA2.

[39] W. Kaiser, editor. *Ultrashort Laser Pulses - Generation and Applications*, volume 60 of *Topics in Applied Physics.* Springer Verlag, New York, 2 edition, 1992.

[40] R. B. Kay and G. S. Waldman. Complete solutions of the rate equations describing Q-spoiled and PTM laser operation. *J. Appl. Phys.*, 36(4):1319–1323, April 1965.

[41] C. J. Kennedy. Cavity-dumping single mode locked pulses from a Nd:YAG laser. *Appl. Opt.*, 15(11):2623–2624, November 1976.

[42] W. R. Klein and B. D. Cook. Unified approach to ultrasonic light diffraction. *IEEE Trans.*, SU-14:123–134, 1967.

[43] H. Kogelnik. Imaging of optical mode-resonators with internal lenses. *Bell Sys. Tech. J.*, 44:455–494, March 1965.

[44] H. Kogelnik, E. Ippen, A. Dienes, and C. V. Shank. Astigmatically compensated cavities for cw dye lasers. *IEEE J. Quantum Electron.*, QE-8(3):373–379, March 1972.

[45] H. Kogelnik and T. Li. Laser beams and resonators. *Proc. IEEE*, 54:1312–1329, October 1966.

[46] P. Lacovara, L. Esterowitz, and M. Kokta. Growth, spectroscopy, and lasing of titanium-doped sapphire. *IEEE J. Quantum Electron.*, QE-21(10):1614–1618, October 1985.

[47] B. E. Lemoff and C. P. J. Barty. Quintic-phase-linited, spatially uniform expansion and recompression of ultrashort optical pulses. *Opt. Lett.*, 18(19):1651–1653, October 1993.

[48] M. Lenzer, C. Spielmann, E. Winter, and F. Krausz. Sub 20fs, kilohertz-repetition-rate Ti:sapphire amplifier. *Opt. Lett.*, 20(12):1397–1399, June 1995.

[49] E. G. Loewen, M. Neviere, and D. Mayste. Grating efficiency theory as it applies to blazed and holographic gratings. *Appl. Opt.*, 16(10):2711–2721, October 1977.

[50] Coherent Laser Group M. K. Reed. Private communication, 1996.

[51] I. H. Malison. Refraction and dispersion of synthetic sapphire. *J. Opt. Soc. Am.*, 525(12):1377, December 1967.

[52] J. H. Marburger. Self-focusing: Theory. *Prog. Quantum Electron.*, 4:35, 1975.

[53] O. E. Martinez. 3000 times grating compressor with positive group velocity dispersion: Application to fiber compensation in 1.3-1.6 μm region. *IEEE J. Quantum Electron.*, QE-23(1):59–64, January 1987.

[54] O. E. Martinez, J. P. Gordon, and R. L. Fork. Negative group velocity dispersion using refraction. *J. Opt. Soc. Am. A*, 1(10):1003–1006, October 1984.

[55] P. Moulton. Spectroscopic and laser characteristics of Ti:sapphire. *J. Opt. Soc. Am. B*, 3(1):125–132, January 1986.

[56] D. K. Negus, L. Spinelli, N. Goldblatt, and G. Feugnet. Sub-100fs pulse generation by Kerr lens mode locking in Ti:Sapphire. In *Proceedings on Advanced Solid-State Lasers*, volume 10, Washington, 1991. Opt. Soc. America.

[57] G. H. C. New. Pulse evolution in mode-locked quasi continuous lasers. *IEEE J. Quantum Electron.*, QE-10:115–124, February 1974.

[58] T. Norris. Femtosecond pulse amplification at 250kHz with a Ti:sapphire regenerative amplifier and application to continuum generation. *Opt. Lett.*, 17(14):1009–1012, July 1992.

[59] T. Norris. Private communication, 1996.

[60] Christopher Palmer. *Diffraction Grating Handbook.* Milton Roy Company, Rochester, NY 14625, 2 edition, 1994.

[61] D. P. Perry and G. Mourou. Terawatt to petawatt subpicosecond lasers. *Science*, 264:917–923, May 1994.

[62] M. Piche and F. Salin. Self mode locking of solid state lasers without an aperture. *Opt. Lett.*, 18(13):1041–1043, July 1993.

[63] M. K. Reed, M. S. Armas, M. K. Steiner-Shepard, and D. K. Negus. 30fs pulses tunable across the visible with a 100kHz Ti:sapphire regenerative amplifier. *Opt. Lett.*, 20(6):605–7, 1995.

[64] M. K. Reed, M. K. Steiner-Shepard, M. S. Armas, and D. K. Negus. Microjoule-energy ultrafast optical parametric amplifiers. *Opt. Lett.*, 12(11):2229–36, 1995.

[65] M. K. Reed, M. K. Steiner-Shepard, and D. K. Negus. Tunable ultraviolet generation using a femtosecond 250 kHz Ti:sapphire regenerative amplifier. *Opt. Lett.*, 31(9):1614–18, 1995.

[66] J. V. Rudd, G. Korn, S. Kane, J. Squier, and Gerard Mourou. Chirped pusle amplification of 55fs pulses at a 1kHz repetition rate in a Ti:sapphire regenerative amplifier. *Opt. Lett.*, 18(23):2044–2046, December 1993.

[67] A. J. Ruggiero, N. F. Scherer, G. M. Mitchell, and G. R. Fleming. Regenerative amplification of picosecond pulses in Nd:YAG at repetition rates in the 100kHz range. *J. Opt. Soc. Am. B.*, 8(10):2061–2067, October 1991.

[68] F. Salin, Jeff Squier, and Gerard Mourou. Multikilohertz Ti:sapphire amplifier for high-power femtosecond pulses. *Opt. Lett.*, 16(24):1964–1966, December 1991.

[69] Y. R. Shen. Self-focusing: Experimental. *Prog. Quantum Electron.*, 4:1, 1975.

[70] Y. R. Shen and G. Z. Yang. Theory of self-phase modulation and spectral broadening. In R. R. Alfano, editor, *The Supercontinuum Light Source*, chapter 1, pages 1–32. Springer Verlag, New York, 1989.

[71] F. Shimizu. Frequency broadening in liquids by a short light pulse. *Phys. Rev. Lett.*, 19:1097, 1967.

[72] A. E. Siegman. Unstable optical resonators for laser applications. *Proc. IEEE*, 53:277–287, March 1965.

[73] A. E. Siegman. *Lasers.* University Science Books, 1986. ISBN 0-935702-11-5.

[74] A. E. Siegman and D. J. Kuizenga. Active mode coupling phenomena in pulsed and continuous lasers. *Opto-electronics*, 6:43–66, 1974.

[75] U. Siegner, M.-A. Mycek, S. Glutsch, and D. S. Chemla. Ultrafast coherent dynamics of Fano resonances in semiconductors. *Phys. Rev. Lett.*, 74(3):470–473, January 1995.

[76] T. M. Smith and A. Korpel. Measurement of light-sound interaction efficiency in solids. *IEEE J. Quantum Electron.*, QE-1:283–284, 1965.

[77] T. S. Sosnowski, P. B. Stephens, and T. B. Norris. Production of 30-fs pulses tunable throughout the visible spectral region by a new technique in optical parametric amplification. *Opt. Lett.*, 21(2):140–2, 1996.

[78] D. Spence, P. Kean, and W. Sibbet. 60fs pulse generation from a self mode locked Ti:sapphire laser. *Opt. Lett.*, 16(1):42–44, January 1991.

[79] B. P. Stoicheff. Characteristics of stimulated raman scattering generated by coherent light. *Phys. Lett*, 7:186, 1963.

[80] R. H. Stolen and C. Lin. Self -phase modulation in silica optical fibers. *Phys. Rev. A*, 17:1448–1453, 1978.

[81] E. B. Treacy. Optical pulse compression with diffraction gratings. *IEEE J. Quantum Electron.*, QE-5(9):454–458, September 1969.

[82] W. E. Lamb, Jr. Theory of an optical maser. *Phys. Rev.*, 134:A1429–A1450, June 1964.

[83] W. Johnston, Jr. and P. Runge. An improved astigmatically compensated resonator for cw dye lasers. *IEEE J. Quantum Electron.*, QE-:724–725, August 1972.

[84] W. G. Wagner and B. A. Lengyel. Evolution of the giant pulse in a laser. *J. Appl. Phys.*, 34:2042–2046, July 1963.

[85] X. D. Wang, P. Basseras, R. J. D. Miller, J. Sweetser, and I. A. Walmsley. Regenerative pulse amplification in the 10kHz range. *Opt. Lett.*, 15:839–841, 1990.

[86] M. U. Wehner, D. Steinbach, and M. Wegener. Three beam four wave mixing on GaAs using 15fs pulses. In *QELS 1996 - Technical Digest*, pages 107–108, Washington, 1996. Optical Society of America.

[87] S. Weiss, M.-A. Mycek, J.-Y. Bigot, S. Schmitt-Rink, and D. S. Chemla. Collective effects in excitonic free induction decay: Do semiconducters and atoms emit coherent light in differnet ways? *Phys. Rev. Lett.*, 69(18):2685–2689, November 1992.

[88] G. Yang and Y.R. Shen. Spectral broadening of ultrashort laser pulses in a nonlinear medium. *Opt. Lett.*, 9:510, 1984.

[89] A. Yariv. Internal modulation in multimode laser oscillators. *J. Appl. Phys.*, 36:388–391, February 1965.

[90] J. Zhou, C.-P. Huang, C. Shi, M. M Murnane, and H. C. Kapteyn. Generation of 21fs millijoule-energy pulses by use of Ti:Sapphire. *Opt. Lett.*, 19(2):126–128, January 1994.

[91] J. Zhou, G. Taft, C.-P. Huang, M. M. Murnane, H. C. Kapteyn, and I. Christov. Pulse evolution in a broad bandwidth Ti:sapphire laser. *Opt. Lett.*, 19(13):1149–1152, June 1994.

Certificate of Originality

Hiermit versichere ich wahrheitsgemäss, die Arbeit bis auf die dem Aufgabensteller bekannten Hilfsmittel selbständig angefertigt, alle Hilfsmittel vollständig angegeben und alles kenntlich gemacht zu haben, was aus Arbeiten anderer unverändert oder mit Abänderungen übernommen worden ist.